LUND UNIVERSITY

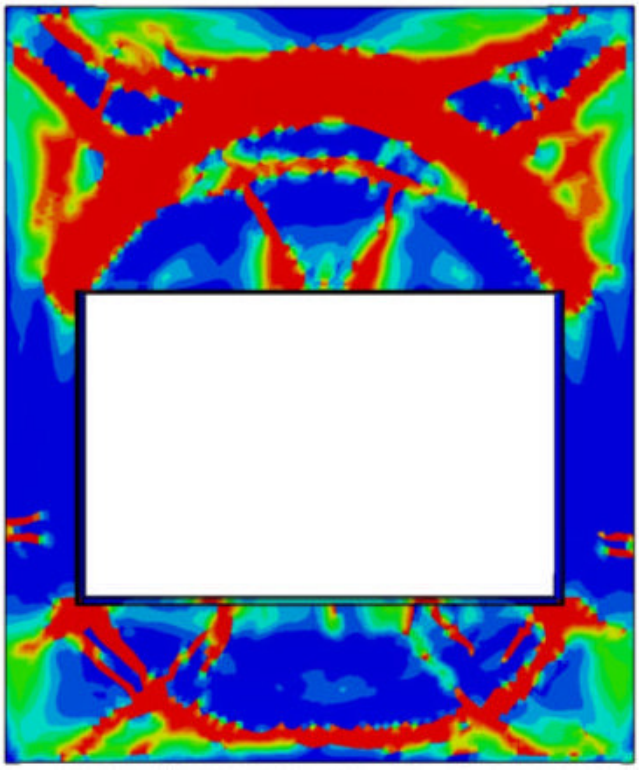

REDUCTION OF EXPLOSION EFFECTS BY USE OF A SANDWICH WALL

ANNIE BOHMAN

Structural Mechanics

Master's Dissertation

DEPARTMENT OF CONSTRUCTION SCIENCES
DIVISION OF STRUCTURAL MECHANICS

ISRN LUTVDG/TVSM--23/5264--SE (1-70) | ISSN 0281-6679
MASTER'S DISSERTATION

REDUCTION OF EXPLOSION EFFECTS BY USE OF A SANDWICH WALL

ANNIE BOHMAN

Supervisors: Professor **KENT PERSSON**, Division of Structural Mechanics, LTH
and **JESPER AHLQUIST**, MSc, Sweco Sverige AB.
Assistant Supervisor: **LINUS ANDERSSON**, Licentiate in Engineering, Division of Structural Mechanics, LTH.
Examiner: **PETER PERSSON**, Associate Professor, Division of Structural Mechanics, LTH.

Printed by V-husets tryckeri LTH, Lund, Sweden, June 2023 *(Pl)*.

For information, address:
Division of Structural Mechanics,
Faculty of Engineering LTH, Lund University, Box 118, SE-221 00 Lund, Sweden.
Homepage: www.byggmek.lth.se

Abstract

It was recently decided that a new hospital is to be built in Växjö. It is important that hospitals can be utilised no matter the circumstances, even in situations of threat. New reports have been published concerning how hospitals are to be designed. In this, it is mentioned that explosions are a threat that should be considered.

Due to this, it was investigated however concrete sandwich walls could lead to less damage to the load carrying part of the wall, when air blasts from an explosion is the considered load. Two different designs of the concrete part were tried, one plate wall element, and one column wall element. Different core materials were also tried; air and phenolic foam of three different stiffnesses.

The problem was numerically simulated by use of the commercial finite element software Abaqus. To compare the different designs, several parameters were analysed. These are: the energy, displacements, tensile damage, reaction force and stress–strain relationship of the reinforcement. From this, it was found out that the most favourable concrete design is when the wall is stiffened by columns. It was also found out that the core that leads to the least damage to the inner wall is air. However, phenolic foam of a low stiffness leads to almost equal results as for air.

Sammanfattning

Det bestämdes nyligen att ett nytt sjukhus skall byggas i Växjö. Det är viktigt att sjukhus kan användas och fungera oberoende av hur världen ser ut, även under oroliga tider. Nya rapporter som anger hur sjukhus bör designas har publicerats. I dessa beskrivs det att explosioner är ett hot som bör tas hänsyn till vid planering och design av sjukhuset.

På grund av detta har betongsandwichväggelement analyserats angående hurvida användning av sådana kan leda till mindre skada för den lastbärande delen av väggen då väggelementet belastas av en luftstötvåg från en explosion. Två olika betonguppbyggnader testades, en med skivformade väggelement, och ett där denna förstärktes med pelare. Även materialet för lagret mellan väggkomponenterna varierades, då luft och fenolskumisolering av varierande styvhet användes.

Problemet löstes via numeriska simuleringar i det finita elementprogrammet Abaqus. För att kunna jämföra de olika uppbyggnaderna valdes några parametrar som undersöktes närmre. Dessa var: energin, förskjutningarna, uppsprickning på grund av drag, reaktionskrafter och spänning–töjningssamband för armeringen. Från detta blev resultatet att den mest gynnsamma betonguppbyggnaden var då innerväggen förstärktes med pelare. Det gick även att avläsa att mellanlagret som leder till minst skada för innerväggen är luft. Dock så sågs det även att fenolskumisolering med en låg styvhet nästan uppnådde samma resultat som för luften.

Acknowledgements

This master's thesis concludes my five years of university studies at Lund University. The work was carried out at the Division of Structural Mechanics, in cooperation with Sweco Sverige AB.

I would like to thank my supervisor from LTH, Prof. Kent Persson, for his help and inputs during the whole process. I would also like to thank my supervisor from Sweco, Jesper Ahlquist, for the initial idea for the thesis, as well as valuable guidance in the startup phase.

Lastly, I would also like to thank my friends and family for supporting me throughout the years.

Lund, June 2023
Annie Bohman

Notations and Abbreviations

Upper Case Letters

E	Young's modulus	[Pa]
I	Impulse	[Ns]
P	Pressure	[Pa]
P_0	Atmospheric pressure	[Pa]
U	Velocity	[m/s]
W	Equivalent mass	[kg TNT]
Z	Scaled distance	[m/kg$^{1/3}$]

Lower Case Letters

i	Impulse	[Pas]
r	Stand-off distance	[m]
t	Duration	[s]
t_a	Arrival time	[s]
t_e	Equivalent duration for triangular model	[s]

Greek Letters

ε	Strain	[−]
ν	Poisson's ratio	[−]
ρ	Density	[kg/m^3]
σ	Stress	[Pa]

Index

$+$	Positive phase
$-$	Negative phase
0	Initial conditions
c	Compression
k	Characteristic value
r	Reflected shock wave
s	Non-reflected shock wave
t	Tension
$\dot{}$	First derivative, velocity/rate
$\ddot{}$	Second derivative, acceleration

Abbreviations

ASE	Artificial Strain Energy
CDP	Concrete Damaged Plasticity
ConWep	Conventional Weapons Effects Programme
CW	Internal work by Constraint Penalty
EW	External Work
FEM	Finite Element Method
G1	Plate wall element
G2	Column wall element
IE	Internal Energy
KE	Kinetic Energy
MSB	Swedish Civil Contingencies Agency
PD	Plastic Dissipation
PF	Phenolic Foam
PW	Internal work by Penalty Contact
SE	Strain Energy
SIS	Swedish Institute for Standards
TE	Total Energy
TNT	Trinitrotoluene
VD	Viscous Dissipation

Contents

1 Introduction

1.1 Background

In March of 2022 it was decided that a new hospital is to be built in Växjö. An important aspect when designing hospitals is that it should be able to function also during war and crisis. In 2021, The Swedish Civil Contingencies Agency (MSB) updated their guidance report for design and planning of hospitals [1]. This report gives guidelines on how a hospital should be built in a way that makes it act robustly against antagonistic attacks, but without stating any specific requirements. In another report by MSB, [2], it is mentioned that sandwich elements can be used favourably against blast loads. Sandwich elements are composite panels built up of several layers, often consisting of a soft core sandwiched between two stiffer outer layers, as shown in Figure 1.1. In this case the stiffer layers consist of concrete walls. These wall elements can be used for resisting explosions since the soft core layer leads to energy being absorbed when the outer concrete plate is pressed towards the inner – load carrying – plate. This would then lead to the load carrying plate being affected by a smaller, more spread out, load. How large effect this would have was not explained further.

1.2 Aim and Objective

The aim of this master's dissertation is to contribute with more knowledge on how blast loads affect concrete sandwich elements. More specifically, to investigate if sacrificing the outer plate and using the layer between the slabs can lead to a reduction of the damage to the inner plate. This will be investigated for sandwich elements of different designs; varying both the geometry of the whole element as well as the material of the mid-layer. These results will then be compared against a solid wall of the same thickness as for the load carrying part of the investigated sandwich wall. The questions that will be investigated are:

- Are sandwich elements favourable in blast loading situations , and what design is in that case the most favourable?
- What methods of analysis are suitable for answering the above questions?

These questions will be investigated by use of the commercial finite element program Abaqus.

1.3 Limitations

Sandwich panels constructed with concrete inner- and outer layers will be analysed. The reason for this is both that the relevant material intended for the hospital project is concrete, but also since the blast load response of sandwich panels with steel or composite sheets already has been analysed more in depth, see for example [3] and [4].

Due to no experiments being conducted for this master's dissertation, the material models are limited to values of earlier documented experiments and studies. Moreover, only chemical explosions due to detonation will be covered.

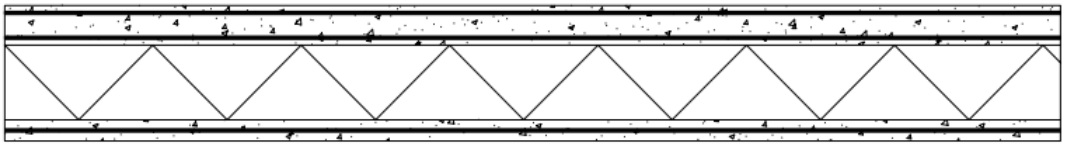

Figure 1.1: A sandwich element

2 Governing Theory

2.1 Blast Loading from Explosions

According to Johansson [5], an explosion is defined by a sudden expansion of matter, which leads to an increase of volume. The explosion leads to the matter going through a change of state, abruptly changing the energy from potential- into mechanical work. There are different ways an explosion can originate, for example as chemical- or mechanical explosions. In this dissertation, only chemical explosions will be covered.

There are two different types of chemical explosions; those initiated by a detonation and those initiated by deflagration. An explosion initiated by a detonation, also called a shock wave, is characterised by its short duration due to the supersonic propagation and a high explosive rate. A deflagration has a longer duration and spreads with subsonic velocity, leading to a lower explosive rate [5]. This sort of phenomena is also called a pressure wave. Following this, only explosions caused by detonations will be covered.

2.1.1 Pressure–Time History

When analysing a structure subjected to a blast load, the explosion is defined in the terms of pressure, impulse and duration. The parameters that influence these the most are presented below.

- The mass and rate of detonation.
- The stand-off distance.
- How the wave is reflected and diffracted.

With an increasing stand-off distance, the amplitude of the pressure and the impulse will decrease, but the duration will increase. This leads to the two bounds: a perfect impulse and a perfect pressure load. In Figure 2.1, a comparison of a characteristic impulse and characteristic pressure is shown.

However, the real load will not be as shown in Figure 2.1 since different factors lead to imperfections. Instead, the history for a fixed point for a stand-off distance r is often represented as shown in Figure 2.2, with a pressure–time history for an idealised explosion. In this figure, there is a positive- and a negative phase, representing the part of the load that is above- and below the ambient atmospheric pressure.

The pressure–time history for the idealised explosion is also shown in Figure 2.3, with notation of the variables used in the dissertation.

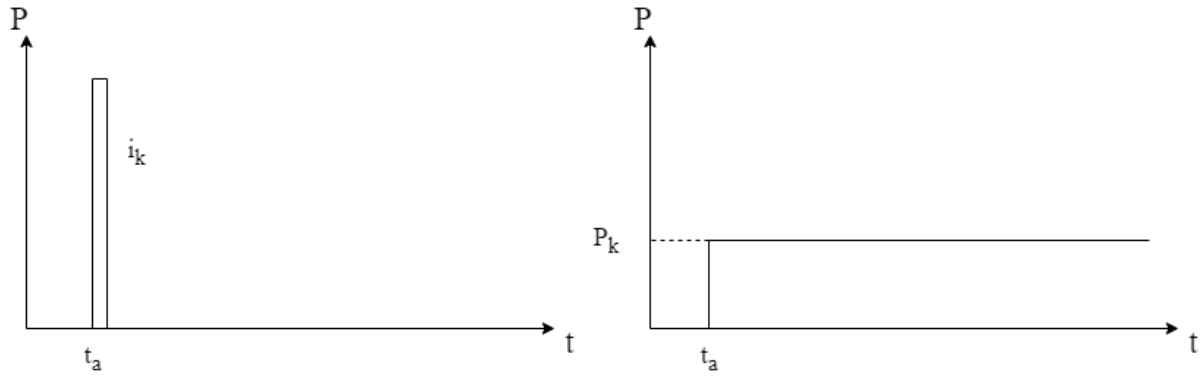

Figure 2.1: Characteristic impulse compared to characteristic pressure, redrawn from [2]

In structural design, the pressure–time history is often simplified into a triangular distribution, with the peak pressure occurring instantly, and then decaying linearly. This means that the negative phase is ignored, which can be done since it is regarded as less damaging than the positive phase [6]. The triangular load model is shown in Figure 2.4.

2.1.2 Regular Reflection and Ground Reflection

According to Johansson and Laine [6], reflection is a phenomenon that drastically influence the properties of the shock wave. There are different types of reflections. In this thesis, only the regular reflection normal to the plane will be explained and used. In Figure 2.5, a schematic figure of the normal reflection is shown, which shows how the conditions differ in front of- and behind the shock wave. The figure to the left represents the undisturbed shock wave travelling towards the wall with the velocity U_p. Behind this wave front, the ambient conditions are determined from the freely

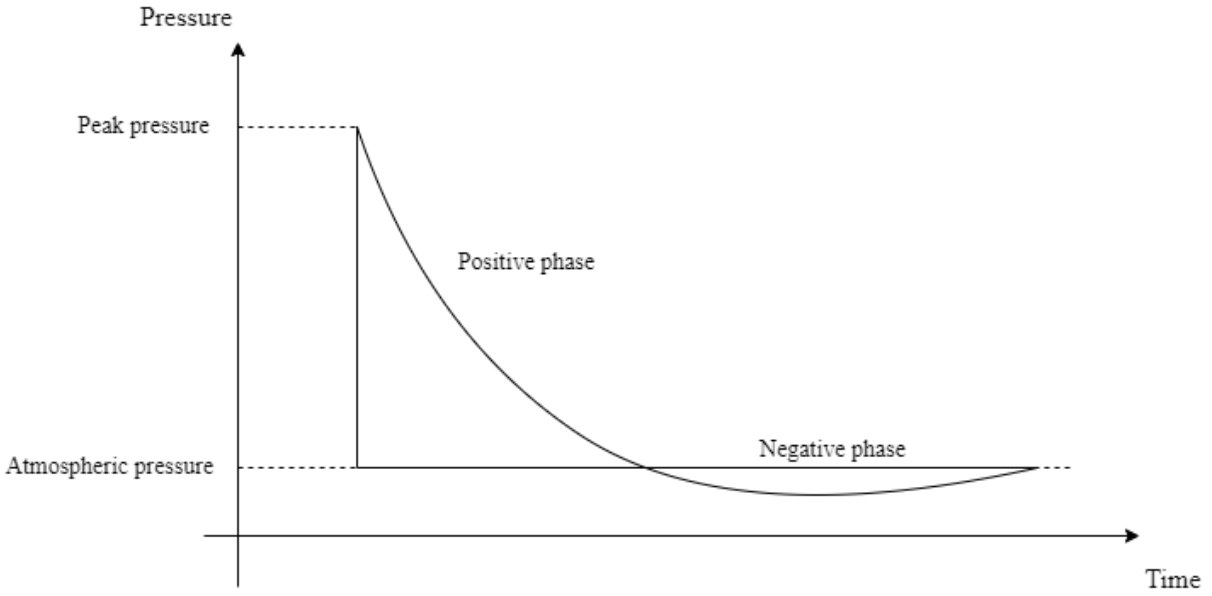

Figure 2.2: Pressure–time history for an idealised explosion, redrawn from [6]

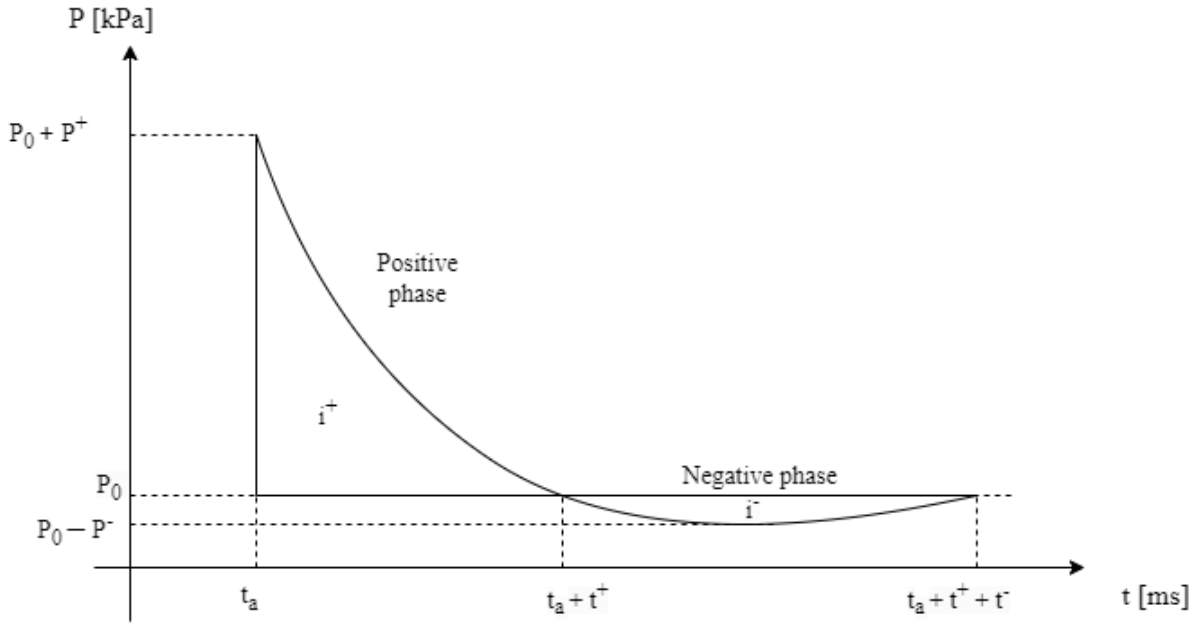

Figure 2.3: Pressure-time history for an idealised explosion, with variables, redrawn from [2]

expanding shock wave, while the conditions in front of the shock wave are undisturbed. To the right, the wave has been reflected off the wall, leading to new conditions. In front of the wave front, the conditions of the non reflected shock wave remain, but behind the wave front, there are new conditions, that often lead to pressures larger than the initial shock wave.

The shock wave will also be affected by the ground. If the detonation originates from

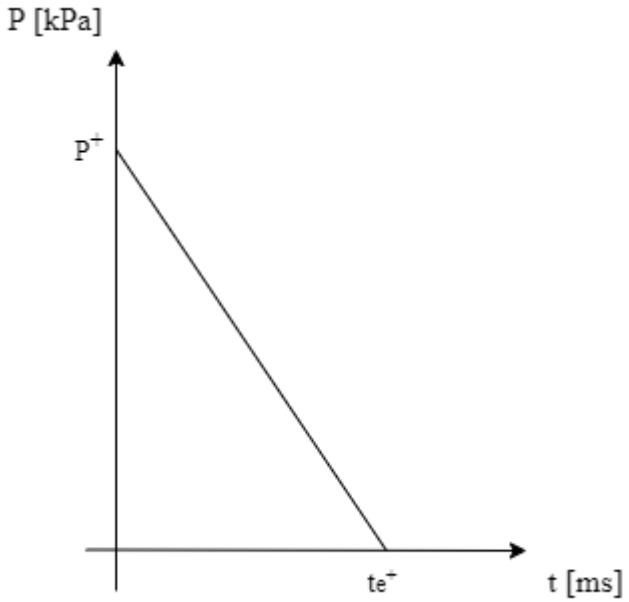

Figure 2.4: Calculation model for the pressure-time history for an idealised explosion, redrawn from [6]

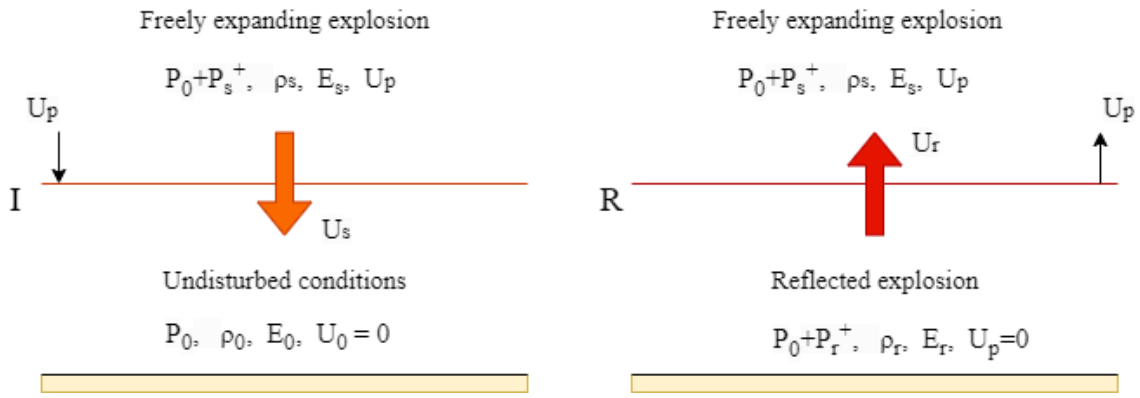

Figure 2.5: Regular reflection, before and after the reflection, redrawn from [6]

the ground level, it can only expand in a half-spherical shape, since it cannot expand down into the ground. This means that the effect of an explosion from the ground level will be larger compared to an explosion that can expand spherically into its surroundings. If it is assumed that no energy is absorbed by the ground, this would mean that the explosion from the ground surface would have the same properties as an explosion of twice the mass, detonating in the free air. This can be illustrated by Figure 2.6.

In real life, however, some of the energy is absorbed by the ground. Due to this, the mass of the charge is not doubled, but instead multiplied with a factor of 1.8 [6].

2.1.3 Scaling Laws

Since the size and properties of an explosion depend both on the mass of the charge, W, as well as the stand-off distance to the investigated point, r, scaling laws are frequently used. The most commonly used one, Hopkinson's scaling law [6], was also used in this dissertation, presented in Equation 2.1. In this equation, Z is the scaled distance.

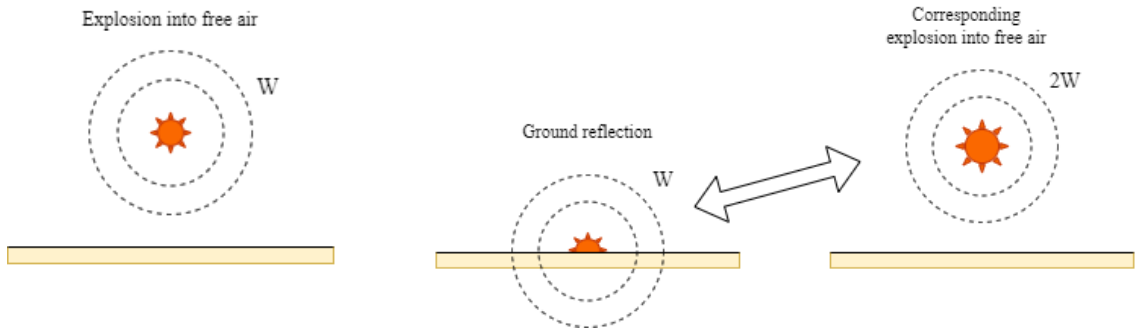

(a) Explosion in air **(b)** Explosion at ground level

Figure 2.6: Ground reflection, redrawn from [6]

$$Z = \frac{r}{W^{1/3}} \tag{2.1}$$

This scaling law means that two explosions will lead to a similar shock wave for stand-off distances proportional to the cubic root of the energy of the respective explosions. This relation is valid for shock waves expanding spherically from a point.

2.1.4 Overpressure and Impulse

Knowing the scaled distance, the overpressure and impulse can be determined by different diagrams. These are presented in Figures 3.13–3.15 in Johansson [6], which in turn is based on the blast simulation software ConWep [7].

2.1.5 Loads

Several different loads may be acting on the wall elements. There is self weight from the building, as well as live load from the utilisation of the hospital. The designing load situation in this thesis, however, is the element's subjection to a blast load. Since this load is much larger than the loads used for designing the wall, only the blast load was accounted for.

Blast Load According to MSB

The size of the blast can be calculated according to the method of MSB presented in [6] and [2]. To determine the size of the impulse, pressure and duration, some input data must be defined. The equivalent mass of the charge was $W = 150$ kg TNT, and the stand-off distance was $r = 15$ m. The factor taking into account the ground reflection, $\alpha = 1.8$, must also be multiplied with the equivalent mass, leading to a modified mass $W_{mod} = \alpha \cdot W = 1.8 \cdot 150 = 270$ kg TNT. With these parameters known, the scaled distance Z can be calculated according to Equation 2.1 as shown below in Equation 2.2.

$$Z = \frac{15}{270^{1/3}} = 2.32\,\mathrm{m/kg^{1/3}} \tag{2.2}$$

Knowing this, the reflected overpressure, P_r^+, can be determined by use of Figure 3.13 in Johansson [6]. This is in turn based on ConWep [7]. Similarly, the reflected impulse, i_r^+, arrival time, t_a, and duration of the positive phase, t^+, can be determined by reading off Figure 3.14 and 3.15 in [6]. The values are presented below in Table 2.1.

The scaled values could be multiplied with the third root of the modified equivalent mass to obtain the actual impulse and times in SI units. These values are presented in Table 2.2.

Table 2.1: Properties of the reflected shock wave, as read from [6]

Property	Symbol	Value	Unit
Reflected overpressure	P_r^+	420	kPa
Scaled reflected impulse	i_r^+	0.20	kPas/kg$^{1/3}$
Scaled arrival time	t_a	2.8	ms/kg$^{1/3}$
Scaled duration	t^+	2.2	ms/kg$^{1/3}$

The impulse may be simplified into a triangular load history, as can be seen in Figure 2.4. The overpressure has the same value as i Table 2.2, but the duration is changed into an equivalent duration, t_e^+. This is done by using Equation E.4 in Johansson and Laine [2], as can be seen below in Equation 2.3.

$$t_e^+ = \frac{2i^+}{P^+} = \frac{2 \cdot 1.29}{420} = 6.16\,\text{ms} \tag{2.3}$$

Due to this, the triangular pressure-time diagram can be drawn as shown in Figure 2.7.

Blast According to the ConWep Module

Abaqus has an implemented module from the blast loading software ConWep [7]. This allows the user to define an incident wave representing the air blast of the explosion. The user can choose how large the mass should be, at what stand-off distance, at what time and how the distribution of the load should be [8]. Abaqus uses ConWep data to define the explosion. In Table 2.3, the input parameters for the module are shown.

The definition of the incident wave was also chosen to be a surface blast, meaning that the load is evenly distributed over the surface of the outer wall.

Table 2.2: Non-scaled properties of the reflected shock wave

Property	Symbol	Value	Unit
Reflected overpressure	P_r^+	420	kPa
Reflected impulse	i_r^+	1.29	kPas
Arrival time	t_a	18.10	ms
Duration	t^+	14.22	ms

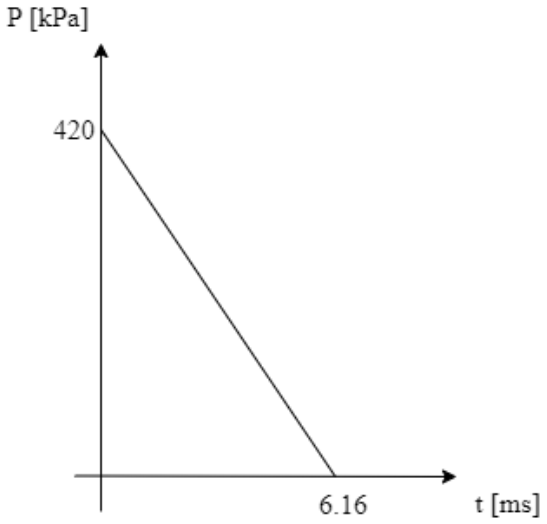

Figure 2.7: The calculated triangular pressure-time history

2.2 Material Models

When analysing a structure affected by a blast load, it is often not possible to statically verify that the load is not larger than the static load capacity. Due to this, one should instead use the deformation capacity of the structure when designing for impulse loads. The energy a structure can absorb depends on its deformation- as well as load capacity. In Figure 2.8, a structure with high stiffness and strength but low deformation capacity is compared to a structure with low stiffness and strength but with high deformation capacity. In this figure, R is the capacity, u is the deformation and W is the energy. This shows that it is oftentime more beneficial to have a structure with a large capacity for deformation than a high stiffness [2].

Since this is an important part on how a structure can withstand a blast load, it is necessary to use realistic models for the materials that accurately portray their plastic behaviour [2]. The finite element software Abaqus was used for the blast simulations, and in this software, there are several material models implemented, some of which were adopted in this work. In the following sections, the theories of the adopted material models will be briefly explained.

Table 2.3: Input parameters for the Abaqus module ConWep

Property	Symbol	Value	Unit
Equivalent mass	W	150	kg TNT
Time of detonation	t_0	0	s

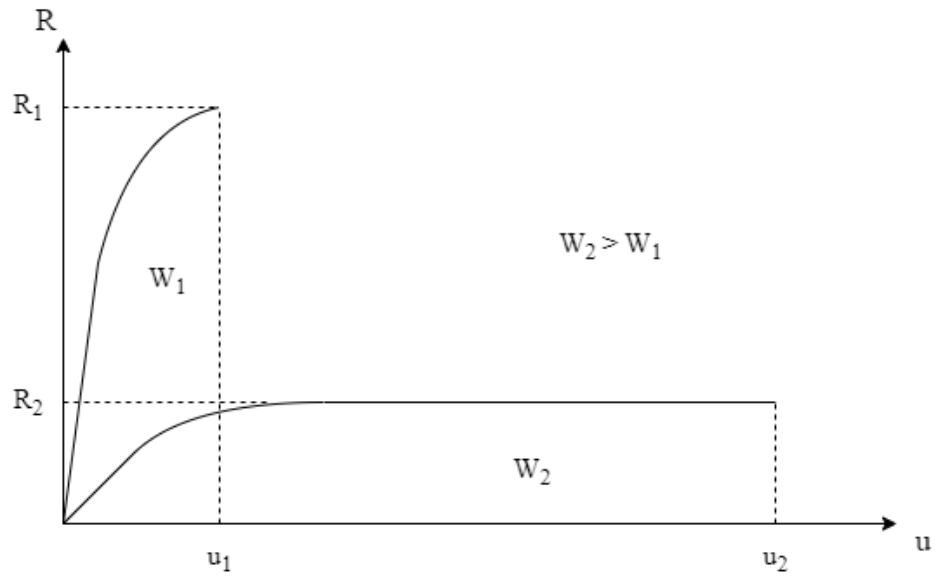

Figure 2.8: Comparison of structure with high stiffness and low deformation capacity to a structure with low stiffness and high deformation capacity redrawn from [2]

2.2.1 Concrete Damage Plasticity

Concrete Damage Plasticity (CDP) is a material model for concrete and other quasi-brittle materials, such as rock, mortar and ceramics [9].

A concrete structure behaves differently based on if it is subjected to a confining pressure or not. If there is no confining pressure, concrete behaves in a brittle way, with cracking in tension and crushing in compression as the main failure mechanisms. If the structure is subjected to a confining pressure, the material behaves in a less brittle way, due to the pressure limiting the crack propagation. Then, the failure mechanisms are dependant on the consolidation and collapse of the micro structure of the concrete, which leads to a response that is alike the hardening of a ductile material [9].

CDP is aimed at concrete structures with low confining pressures, and thus captures the failure mechanisms of this type of loading. The important properties for this model can be presented below [9].

- Different yield strength in compression and tension.
- Tension softening behaviour.
- Different degradation of elastic stiffness in compression and tension.
- Dependant on the strain rate sensitivity.

Strain Rate

The strain rate is assumed to be additive as shown in Equation 2.4, in which the total strain rate is comprised of the elastic and plastic strain rate.

$$\dot{\varepsilon} = \dot{\varepsilon}^{el} + \dot{\varepsilon}^{pl} \tag{2.4}$$

Stress–Strain Relationship

The stress–strain relationship is determined by scalar damaged elasticity, as shown in Equation 2.5.

$$\boldsymbol{\sigma} = (1-d)\boldsymbol{D}_0^{el} : (\varepsilon - \varepsilon^{pl}) = \boldsymbol{D}^{el} : (\varepsilon - \varepsilon^{pl}) \tag{2.5}$$

In this equation, the damage parameter, d, can take on a value between 0 and 1, where an increasing value means increasing damage. $\boldsymbol{D}_0^{el}$ is the initial elastic stiffness of the material, and ε is the strain.

In Equation 2.6, the effective stress is defined.

$$\bar{\boldsymbol{\sigma}} \overset{def}{=} \boldsymbol{D}_0^{el} : (\varepsilon - \varepsilon^{pl}) \tag{2.6}$$

Further, the formula for the stress can be rewritten by combining Equations 2.5 and 2.6, resulting in Equation 2.7.

$$\boldsymbol{\sigma} = (1-d)\bar{\boldsymbol{\sigma}} \tag{2.7}$$

Hardening

Tensile and compressive damage is comprised of two variables appointed equivalent plastic strain. The strains can be calculated as shown in Equation 2.8.

$$\tilde{\boldsymbol{\varepsilon}}^{pl} = \begin{bmatrix} \tilde{\varepsilon}_t^{pl} \\ \tilde{\varepsilon}_c^{pl} \end{bmatrix}; \qquad \dot{\tilde{\boldsymbol{\varepsilon}}}^{pl} = \boldsymbol{h}(\bar{\boldsymbol{\sigma}}, \tilde{\boldsymbol{\varepsilon}}^{pl}) \cdot \dot{\boldsymbol{\varepsilon}}^{pl} \tag{2.8}$$

$\tilde{\boldsymbol{\varepsilon}}^{pl}$ is the equivalent plastic strain.

Yield Function

The yield function defines a surface in the effective stress space, in which the failure is determined. This is presented in Equation 2.9.

$$F(\bar{\boldsymbol{\sigma}}, \tilde{\boldsymbol{\varepsilon}}^{pl}) \leq 0 \tag{2.9}$$

Flow Rule

The plastic flow is defined by Equation 2.10 below. This is non-associated, meaning that the yield function and the plastic potential do not coincide, and the direction of the plastic flow is thus not normal to the yield surface [10].

$$\dot{\boldsymbol{\varepsilon}}^{pl} = \dot{\lambda} \frac{\partial G(\bar{\boldsymbol{\sigma}})}{\partial \bar{\boldsymbol{\sigma}}} \tag{2.10}$$

G is the flow potential, $\dot{\lambda}$ is the non-negative plastic multiplier.

Damage

The uniaxial tensile and compressive stress–strain relations can be defined as shown in Equations 2.11 and 2.12, respectively.

$$\sigma_t = (1 - d_t) E_0 (\varepsilon_t - \tilde{\varepsilon}_t^{pl}) \tag{2.11}$$

$$\sigma_c = (1 - d_c) E_0 (\varepsilon_c - \tilde{\varepsilon}_c^{pl}) \tag{2.12}$$

E_0 is the undamaged Young's modulus, and the damage parameters are dependant on the equivalent plastic strain.

Input Parameters

The planned concrete strength class of the sandwich panels is C50/60. The concrete was modelled using elasticity combined with the in Abaqus implemented material model CDP. In Table 2.4, the density, Young's modulus and Poisson's ratio for the concrete are shown.

The data used in the CDP part of the model was taken from Hafezolghorani et al. [10], Table 4. This data has been used in Abaqus earlier for simulations with high strain rate, see for example [12]. In Table 2.5, the input data for the CDP model is

Table 2.4: Properties for the concrete

Property	Symbol	Value	Unit
Density [11]	ρ	2500	kg/m^3
Young's modulus [10]	E	33.4	GPa
Poisson's ratio [10]	ν	0.2	–

presented. Used for the model is also measured values for compression and tension, that can be found in [10].

2.2.2 Metal Plasticity

The reinforcement also has to be adequately considered in a reinforced concrete model. This was done by the use of a von Mises plastic material model with isotropic hardening and associated plastic flow [8]. The model is presented in the section below with derivations from the Abaqus Theory Manual [9].

Theory

In Equation 2.13, the isotropic hardening is defined.

$$f(\boldsymbol{\sigma}) = \sigma^0(\varepsilon^{pl}, \theta) \tag{2.13}$$

$$\sigma^0 \dot{\varepsilon}^{pl} = \boldsymbol{\sigma} : \dot{\boldsymbol{\varepsilon}}^{pl} \tag{2.14}$$

σ^0 is the equivalent uniaxial stress, ε^{pl} is the plastic strain defined as shown in Equation 2.14, and θ is the temperature.

Input Parameters

The reinforcement, chosen to be of strength class B500B was modelled as a linearly hardening elastoplastic material. It is assumed that the concrete cover is $c = 25$ mm. The density, Young's modulus and Poisson's ratio used for the reinforcement are shown in Table 2.6.

Table 2.5: Properties for CDP

Dilation angle	Eccentricity	f_{b0}/f_{c0}	K	Viscosity parameter
31°	0.1	1.16	0.67	0.0

Table 2.6: Properties for the reinforcement

Property	Symbol	Value	Unit
Density [13]	ρ	7850	kg/m^3
Young's modulus [14]	E	200	GPa
Poisson's ratio [14]	ν	0.3	–

The plastic part of the stress strain relationship of the reinforcement was modelled using the Mises yield surface, which is an isotropic model. With this model it is assumed that the metal yields independently of the equivalent pressure stress. The values used are shown in Table 2.7, and these are taken from the Swedish Institute for Standards (SIS) [13].

2.2.3 Crushable Foam

Crushable foam is a material model for analysis of foams. There are two versions, the volumetric- and isotropic hardening models, of which both use a yield surface elliptically dependant of deviatoric stress on pressure stress in the meridional plane. The volumetric hardening model has different behaviour depending on if the structure is loaded in compression or tension. The isotropic hardening model behaves in the same way for both loading situations [9].

The model with volumetric hardening was adopted in this work. The model is presented in the section below with derivations from the Abaqus Theory Manual [9].

Elastic Behaviour

The elastic part is modelled as linear elastic, shown in Equation 2.15.

$$\boldsymbol{\sigma} = \boldsymbol{D}^{el} : \varepsilon^{el} \tag{2.15}$$

$\boldsymbol{D}^{el}$ is the fourth order elasticity tensor.

Table 2.7: Plastic property values for the reinforcement

	Stress [MPa]	Strain [%]
Yield	f_{yk}=500	0
Failure	f_{tk}=540	5

Plastic Behaviour

The von Mises yield surface is defined as shown in Equation 2.16.

$$p = -\frac{1}{3}\,\mathrm{trace}\,\boldsymbol{\sigma} = -\frac{1}{3}\boldsymbol{\sigma} : \boldsymbol{I} \tag{2.16}$$

Also, the von Mises stress can be defined as Equation 2.17 shows.

$$q = \sqrt{\frac{3}{2}\boldsymbol{S} : \boldsymbol{S}} \tag{2.17}$$

$\boldsymbol{S}$ represents the deviatoric stress components, defined as $\boldsymbol{S} = \boldsymbol{\sigma} + p\boldsymbol{I}$.

Yield Surface

The yield surface for the volumetric hardening crushable foam model is shown in Equation 2.18. This is defined in pressure stress.

$$F = \sqrt{q^2 + \alpha^2(p - p_0)^2} - B = 0 \tag{2.18}$$

α is a shape factor for the shape of the ellipse that defines the yielding. k and k_t are yield stress ratios. These are defined in Equation 2.19. For the yield surface to be valid, the values should be defined so that $0 < k < 3$ and $k_t \geq 0$. These variables are defined in Equation 2.19.

$$\alpha = \frac{3k}{\sqrt{(3k_t + k)(3 - k)}}; \qquad k = \frac{\sigma_c^0}{p_c^0}; \qquad k_t = \frac{p_t}{p_c^0} \tag{2.19}$$

In this, σ_c^0 is the initial yield strength in uniaxial compression, p_c^0 is the initial yield strength in hydrostatic compression and p_t is the yield strength in hydrostatic tension. In Equation 2.20, the parameters p_0 and B are defined. These, respectively, represent the mid point and height of the yield ellipse, see Figure 2.9.

$$p_0 = \frac{p_c - p_t}{2} \qquad B = \alpha\frac{p_c + p_t}{2} \tag{2.20}$$

It is assumed that the tensile hydrostatic yield strength, p_t, is constant. However, the hydrostatic compressive yield strength is dependant on the strain in a way shown in Equation 2.21.

$$p_c = p_c(\bar{\varepsilon}), \qquad \text{in which} \qquad \bar{\varepsilon} = -\mathrm{trace}(\varepsilon^{pl}) \tag{2.21}$$

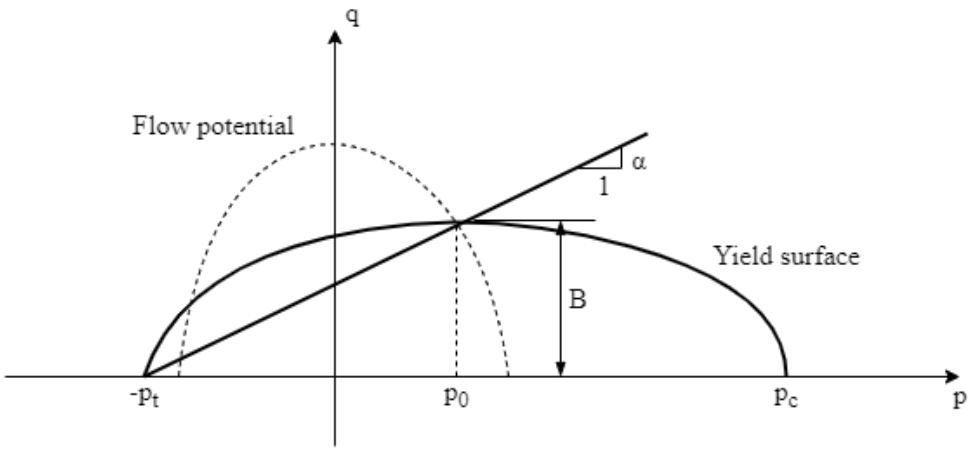

Figure 2.9: Yield surface- and flow potential ellipse, redrawn from [9]

Flow Potential

The plastic strain rate is defined as shown in Equation 2.22.

$$\dot{\boldsymbol{\varepsilon}}^{pl} = \dot{\bar{\varepsilon}}^{pl} \frac{\partial G}{\partial \boldsymbol{\sigma}} \tag{2.22}$$

$\dot{\bar{\varepsilon}}^{pl}$ is the equivalent plastic strain rate that can be defined as shown in Equation 2.23.

$$\dot{\bar{\varepsilon}}^{pl} = \frac{\boldsymbol{\sigma} : \dot{\boldsymbol{\varepsilon}}^{pl}}{G} \tag{2.23}$$

G is the chosen flow potential, that can be written as shown in Equation 2.24.

$$G = \sqrt{q^2 + \beta^2 p^2} \tag{2.24}$$

In this, β is a factor representing the shape of the flow potential ellipse.

Hardening

The hardening of the material can be defined as shown in Equation 2.25. The evolution of the yield surface can be defined by the change of size of the hydrostatic stress axis, as a function of the volumetric compacting strain.

$$p_c(\varepsilon^{pl}_{vol}) = \frac{\sigma_c(\varepsilon^{pl}_{axial})[\sigma_c(\varepsilon^{pl}_{axial})(\frac{1}{\alpha^2} + \frac{1}{9}) + \frac{p_t}{3}]}{p_t + \frac{\sigma_c(\varepsilon^{pl}_{axial})}{3}} \tag{2.25}$$

Input Parameters

The foam material chosen to represent the insulation layer was phenolic foam (PF). Phenolic foams are made by foaming and curing a phenolic resin configuration, created of phenolic resin, a blowing agent, an acid catalyst and inorganic filler [15]. The result is a rigid cellular foam with mostly closed cells, with a lower limit of 90% closed cells, according to SIS [16]. The foam works well as thermal insulation, and also has an effective fire retardant behaviour, however, of most interest in this dissertation, is that it also has energy absorbing capabilities [17].

The values used were obtained from [18], and are presented below in Table 2.8. Here, the compression- and hydrostatic yield stress ratio are input parameters for the Crushable foam material model.

In the Crushable foam model, the yield stress and corresponding uniaxial plastic strain is needed as input. In [18], results from uniaxial compressive tests, and measurements of the stress as well as the strain are presented. The nominal strain was used for calculating the uniaxial logarithmic plastic strain according to Equation 2.26.

$$\varepsilon^{pl}_{axial} = \ln(1 + \varepsilon_{nom}) - \varepsilon^{el} \tag{2.26}$$

This led to the values being used in the material model as seen in Table 2.9.

2.2.4 Air

To adequately represent the air in the model, it was modelled as a pneumatic fluid cavity as well as with acoustic elements. The fluid cavity model assumes that the contained gas is an ideal gas [8]. From use of this method, the volume- and gauge pressure history for the cavity can be extracted during the analysis. Acoustic elements only register pressure and pressure waves [19]. The results of these two ways of modelling the air were then compared to the results of a model in which the cavity between the inner- and outer walls was left empty.

In Table 2.10 below, with values from Wadsö [20], the properties used for the air are shown.

Table 2.8: Properties for PF

Property	Symbol	Value	Unit
Density	ρ	120	kg/m^3
Young's modulus	E	27	MPa
Poisson's ratio	ν	0.1	–
Initial uniaxial compressive yield stress	σ_{c0}	0.4	MPa
Compression yield stress ratio	k	1.0	–
Hydrostatic yield stress ratio	k_t	0.1	–

Table 2.9: Yield stress and uniaxial plastic strain for PF

Yield stress [MPa]	Uniaxial plastic strain [%]
0.375	0
0.42	1.44
0.38	13.70

Needed for explicit calculations was also the molar heat capacity for the air. This was implemented as a polynomial model as can be seen in Equation 2.27 [19].

$$\tilde{c}_p = \tilde{a} + \tilde{b}(\theta - \theta^Z) + \tilde{c}(\theta - \theta^Z)^2 + \tilde{d}(\theta - \theta^Z)^3 + \frac{\tilde{e}}{(\theta - \theta^Z)^2} \tag{2.27}$$

$\tilde{a} - \tilde{e}$ are gas constants, θ is the temperature and θ^Z is the absolute zero temperature. The gas constants are presented in Table 2.11, with the values from the Abaqus Analysis User's Guide [19].

2.3 Numerical Approximation

Due to the fact that the stated problem is too complex to be solved with analytical calculations, numerical approximations were utilised. This was done by use of the finite element method (FEM), which is a method of dividing the structure into smaller parts, and approximating the solution for each of these finite elements (FE) [21]. The computational simulations were done by using the commercial FE software Abaqus. For solving this problem, the explicit analysis method was utilised.

The explicit method solves the problem without use of equilibrium conditions. The values for the new time step are directly solved for by using the previously known variables. This causes the method to be computationally fast, but with a risk of it becoming unstable and inaccurate if the time increments are too large. In this section, the Central difference method will be presented, with derivations based on Chopra [22].

Table 2.10: Properties of air

Property	Value	Unit
Air pressure, P_0	101.325	kPa
Bulk modulus	101.325	kPa
Molecular weight	28.9647	g/mol
Density, ρ_0	1.293	kg/m^3
Universal gas constant	8.314	J/molK

Table 2.11: Molar heat conductivity of air

Symbol	Value
$\tilde{a}$	28.110
$\tilde{b}$	$1.967 \cdot 10^{-3}$
$\tilde{c}$	$4.802 \cdot 10^{-6}$
$\tilde{d}$	$-1.966 \cdot 10^{-9}$
$\tilde{e}$	0

2.3.1 Central Difference Method

The equation of motion can be written as shown in Equation 2.28.

$$m\ddot{u}_i + c\dot{u}_i + ku_i = p_i \tag{2.28}$$

According to the Central difference method, the velocity and acceleration at the time i can be expressed as shown below in Equations 2.29 and 2.30.

$$\dot{u}_i = \frac{u_{i+1} - u_{i-1}}{2\Delta t} \tag{2.29}$$

$$\ddot{u}_i = \frac{1}{(\Delta t)^2}(u_{i+1} - 2u_i + u_{i-1}) \tag{2.30}$$

The equation of motion can then be rewritten by inserting Equations 2.29 and 2.30 into Equation 2.28, leading to Equation 2.31.

$$m\frac{u_{i+1} - 2u_i + u_{i+1}}{(\Delta t)^2} + c\frac{u_{i+1} - u_{i-1}}{2\Delta t} + ku_i = p_i \tag{2.31}$$

The displacements u_i and u_{i-1} are assumed to be known, and therefore the unknown displacement u_{i+1} can be solved for as shown in Equation 2.32.

$$u_{i+1} = \hat{k}^{-1}\hat{p}_i \tag{2.32}$$

In this expression, $\hat{p}_i$ and $\hat{k}$ can be defined as shown below in Equations 2.33 and 2.34.

$$\hat{p}_i = p_i + \left[\frac{m}{(\Delta t)^2} - \frac{c}{2\Delta t}\right]u_{i-1} - \left[k - \frac{2m}{(\Delta t)^2}\right]u_i \tag{2.33}$$

$$\hat{k} = \frac{m}{(\Delta t)^2} + \frac{c}{2\Delta t} \tag{2.34}$$

To be able to start the iterative process, $u_{i+1} = u_1$, $u_i = u_0$ and $u_{i-1} = u_{-1}$ are needed. u_0 is assumed to be known, but u_{-1} needs to be determined. This is done by using Equations 2.29 and 2.30, with $i = 0$ as the time, which is shown in Equation 2.35.

$$\dot{u}_0 = \frac{u_1 - u_{-1}}{2\Delta t} \qquad \ddot{u}_0 = \frac{u_1 - 2u_0 + u_{-1}}{(\Delta t)^2} \tag{2.35}$$

u_{-1} can then be expressed as shown below in Equation 2.36.

$$u_{-1} = u_0 - \Delta t(\dot{u}_0) + \frac{(\Delta t)^2}{2}\ddot{u}_0 \tag{2.36}$$

Now, the initial values of the displacement and velocity are known, and therefore the initial acceleration can be solved for by use of Equation 2.28. The result is shown in Equation 2.37.

$$\ddot{u}_0 = \frac{p_0 - c\dot{u}_0 - ku_0}{m} \tag{2.37}$$

Use of the Central difference method will become unstable if a too large time step is used. Therefore there is a requirement for stability, which is presented in Equation 2.38.

$$\frac{\Delta t}{T} \leq \frac{1}{\pi} \tag{2.38}$$

However, the fact that the system is stable does not mean that it leads to accurate results. Therefore, a smaller time step than this limit should be used.

2.3.2 Energy

When doing explicit analyses, it is important to check the energies, so that the internal- and external energies are not diverging. That is a sign of something in the analysis going wrong. There are also other problematic signs to watch out for. Some of them are presented below [19].

- Total energy not being relatively constant.
- Large negative strain energy.
- "Artificial" energies being large compared to the "real" energies.
- Constraint- and contact energies not being close to zero.

3 Numerical Modelling and Analyses

The sandwich element was modelled in the FE software Abaqus. In this chapter, the modelling will be described.

3.1 Performed Analyses

In total, 28 different models were analysed. There were two versions of applying the load, as described in Chapter 2.1.5, two different geometries for the concrete part of the wall, as well as seven versions of each geometry: three different ways of modelling the air, three different phenolic foams and one solid wall. The geometries are described in more detail in Chapter 3.2.

The results that were extracted after the analyses were:

- Energy metrics.
- Displacement of the inner- and outer slabs.
- Tensile damage of the concrete.
- How large of a reaction force that is transferred into the rest of the building.
- Stress and strain of the reinforcement.

These results were then investigated to conduct several comparisons and evaluations. These are presented below.

- Comparison of a sandwich design to a solid wall.
- Comparison of MSB- and ConWep load for the same geometry.
- Comparison of the concrete geometries.
- Comparison of ways to model air.
- For the sandwich design with phenolic foam, what stiffness is optimal?

3.2 Geometry

Various geometries and designs of the sandwich panels were investigated. Both the geometry as well as the material of the core were varied. Two different types of wall elements were studied, the plate–wall element and the column–wall element, presented in the following section. The investigated core materials between the outer and inner walls were phenolic foam of three different stiffnesses, as well as air modelled in three different ways.

3.2.1 Sandwich Element

The size of the wall element was constant in the plane but the geometry of the cross section was varied. The dimensions of the wall elements are from an existing hospital project. The elements that were modelled are the plate–wall element, also denoted G1 (Geometry 1), and the column–wall element, also denoted G2 (Geometry 2). These are shown in Figures 3.1 and 3.2.

3.2.2 Cross Section

The core materials were varied to investigate which one had the best resistance to blast loads. In Figure 3.3, the plate–wall element is shown and in Figure 3.4 the column–wall element is shown. For this geometry, the core material was varied as for the other design.

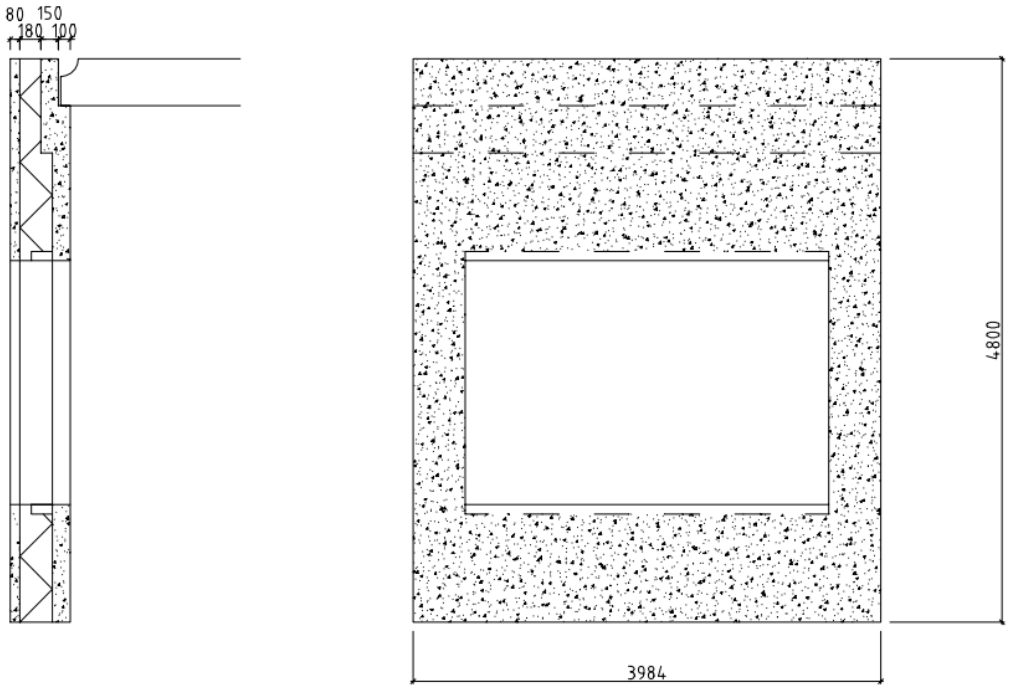

Figure 3.1: Plate–wall element, section and from the front

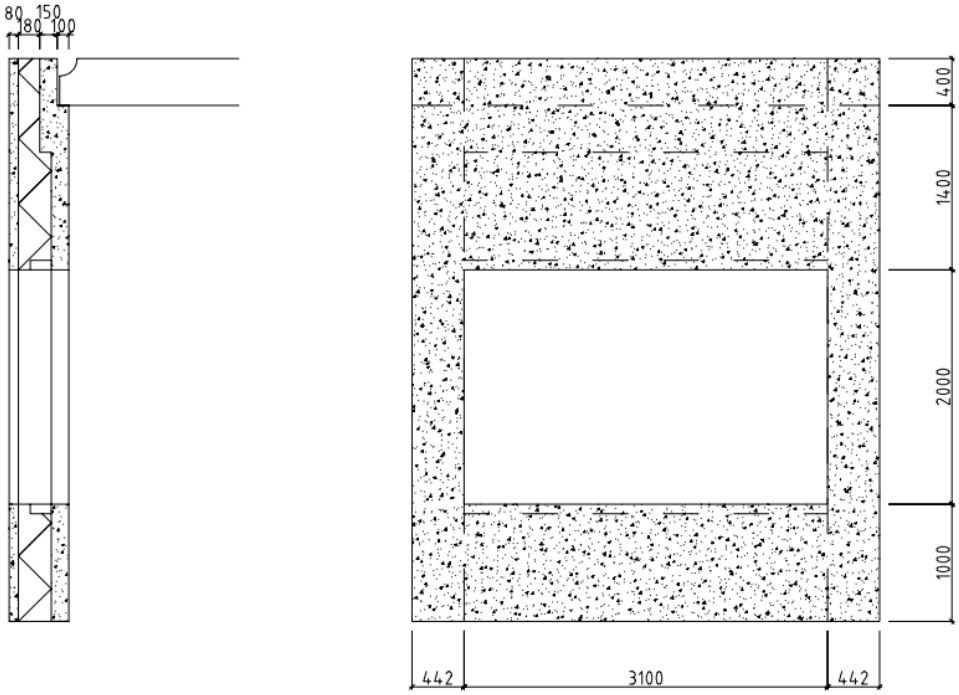

Figure 3.2: Column–wall element, section and from the front

3.2.3 Core Materials

The different wall designs, and what core material was used for these, is presented in the sections below.

Inner Wall Only

To observe if the sandwich design is favourable at all when the wall is affected by a blast load, a control model was made. This consisted of the inner wall only, to be able to compare the sandwich design with a solid wall. In the results, this will be denoted 'Inner only'.

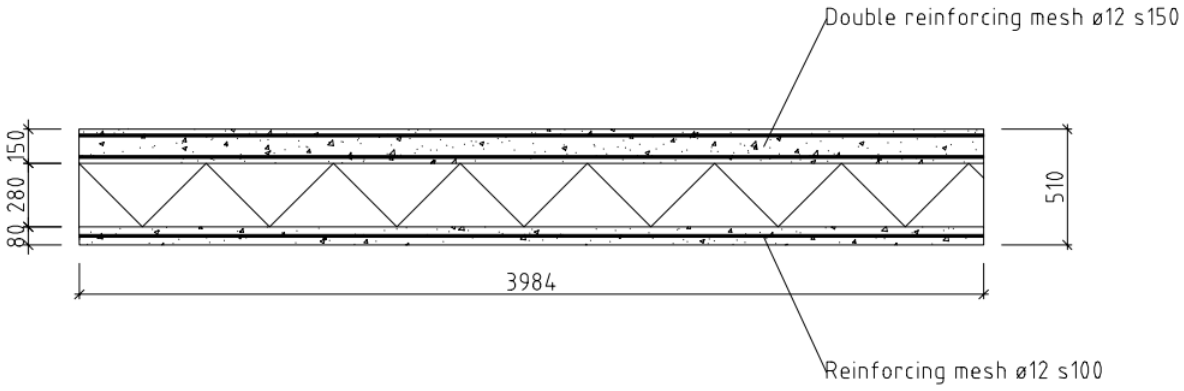

Figure 3.3: Plate–wall element proposal

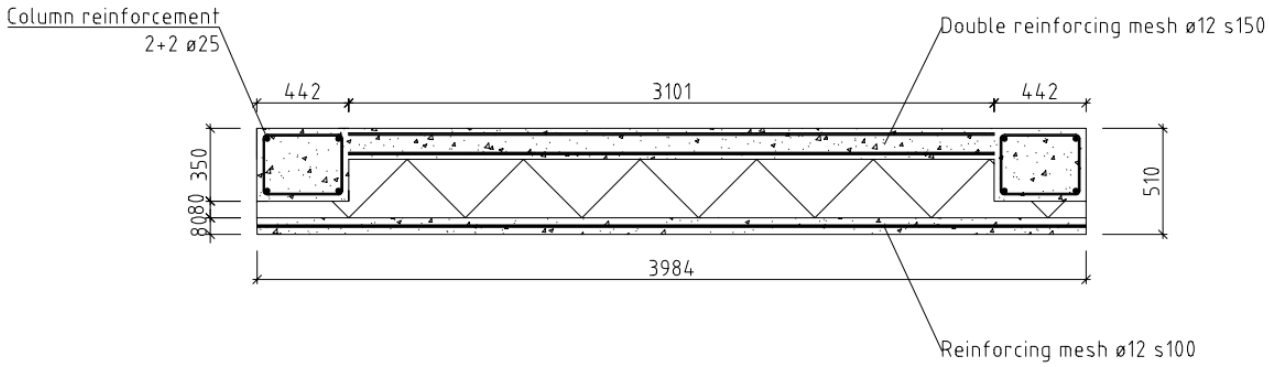

Figure 3.4: Column–wall element proposal

Phenolic Foam

Phenolic foam was used to represent the insulation. To analyse how the foam affects the behaviour of the wall, different stiffnesses were used. In Chapter 2.2.3, the Young's modulus for the actual foam is shown to be 27 MPa, but to easily compare how the stiffness affects the behaviour of the structure, 2.7 MPa and 0.27 MPa were also used, with the other properties kept constant. In the results, these models will be denoted 'PF, E=27 MPa', 'PF, E=2.7 MPa' and 'PF, E=0.27 MPa', respectively.

Air

The air was modelled in three different ways: with a fluid cavity, with acoustic elements and with an empty cavity. In the results, these models will be denoted 'Fluid cavity', 'Acoustic' and 'Empty', respectively.

3.2.4 Modelling of the Plate–Wall Element

In Figure 3.5, the FE geometry for the plate–wall element – first presented as design drawings in Figures 3.1 and 3.3 – is shown. The concrete slabs were modelled with 3D deformable four node shell elements, and the reinforcement was in this section accounted for by use of a smeared rebar layer. The geometry was simplified somewhat as compared to Figure 3.1, since the top part was modelled without the notch.

The inner and outer slabs were connected by the use of elements with increased stiffness, placed as a frame around the whole structure. There were several reasons why these stiff elements were used; firstly to prevent the outer slab to move with a rigid body motion once the blast load hit, by connecting the slabs to each other and secondly to be able to model the air as a closed fluid cavity. Around the window opening, concrete elements of a lesser stiffness were added.

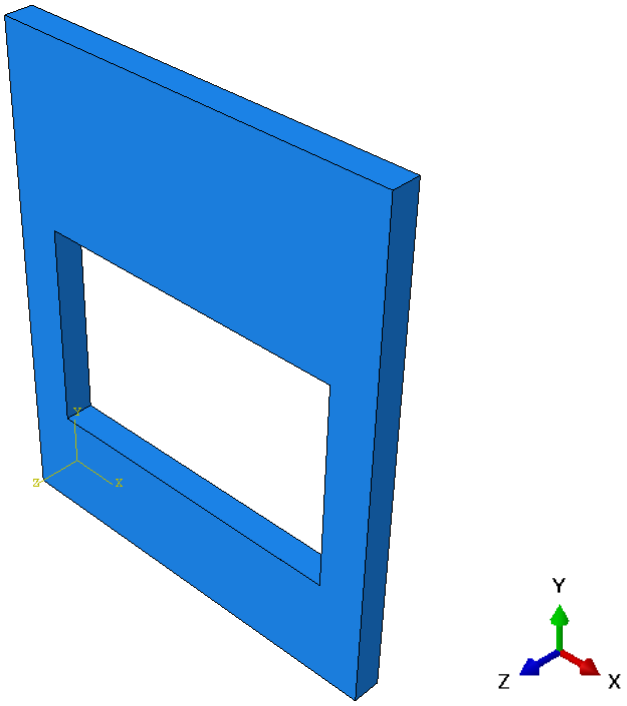

Figure 3.5: The plate–wall element in Abaqus

3.2.5 Modelling of the Column–Wall Element

The FE geometry of the column–wall element – first presented in Figures 3.2 and 3.4 as design drawings – is shown in Figure 3.6. The slabs were modelled in the same way as the first geometry, but the columns were modelled by use of solid elements, with the reinforcement added as embedded wires. As for the first geometry, this geometry was simplified somewhat, since the top part was assumed to be without the notch.

For this model as well, the inner- and outer slabs were connected by use of stiff elements in a frame around the wall element. Around the windows, the same type of concrete elements as for the first model were also used.

3.3 Boundary Conditions

The boundary conditions used are shown in Figure 3.7. The inner lines of the inner wall were prescribed to zero in the Z-direction, since it in the real construction will be connected to the rest of the building, and therefore will have little possibility for movement. To avoid rigid body motion, a node in the bottom corner was prescribed to zero in the X- and Y-direction. Lastly, to avoid a rotation of the element, a point in the opposite corner was prescribed to zero in the y-direction.

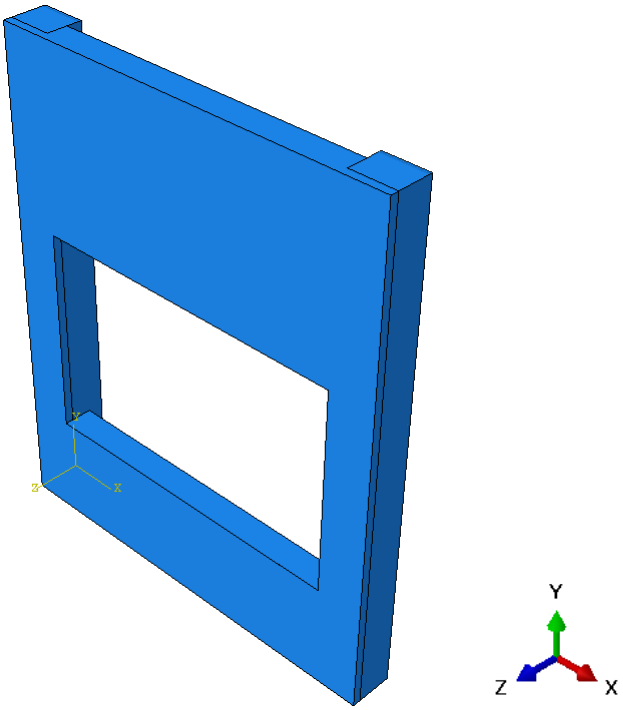

Figure 3.6: The column–wall element in Abaqus

3.4 Structural Interactions

To connect the different parts together, constraints were used along the outer lines of each part. The connections between the shell element were modelled with 'Ties',

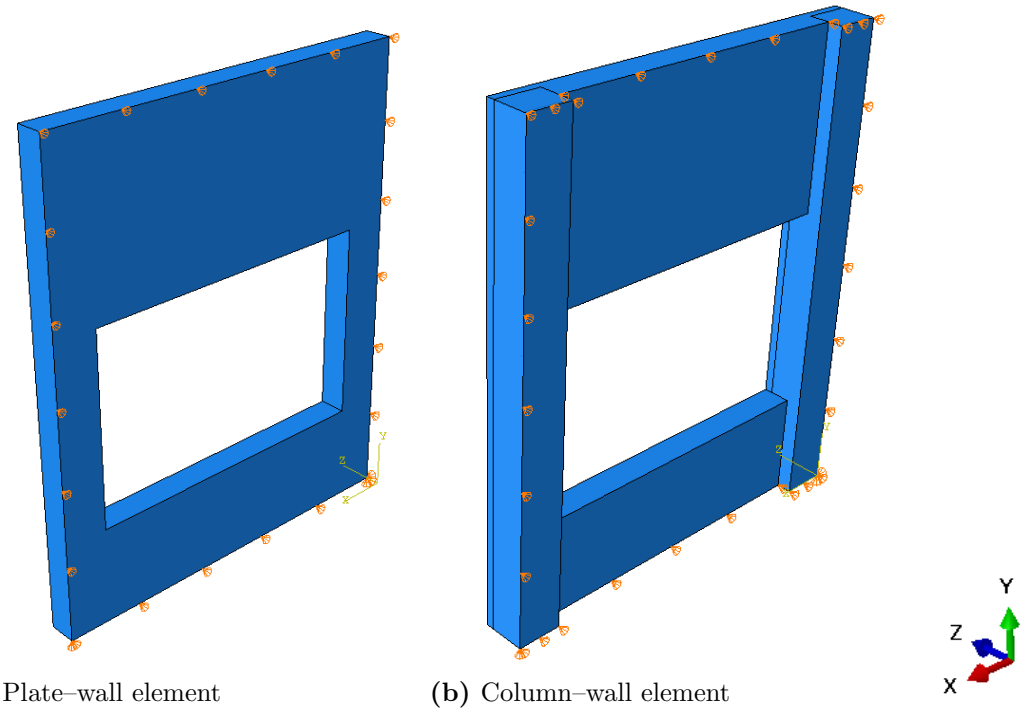

(a) Plate–wall element **(b)** Column–wall element

Figure 3.7: Boundary conditions

meaning that there is allowed no relative motion between the parts in question [8]. The connection between the solid column and the shell slab was modelled with so called 'Shell-to-solid couplings' between the edge of the shell element, and the surface of the column. These connections connect the displacements and rotations of the shell to the displacements and rotations of the solid [19]. As before mentioned, the reinforcement was connected to the column as 'Embedded elements'.

Contact was defined for the whole model as a general contact, using the default properties. The assumptions for this model are for example "hard" contact in the normal direction and no friction [19]. Contact was defined so that the deformations of the concrete- and foam parts would affect each other if contact occurred.

3.5 Loads

The blast load calculated in Chapter 2.1.5 was used for the modelling. In Figure 3.8, the loads affecting the sandwich elements are shown. This load type was added as a pressure on the surface of the outer slab as a function over time.

In Table 3.1, the duration and load used for the linearly decreasing pressure load with time is shown. These values correspond to the earlier presented Figure 2.7.

The load was also added by use of an incident wave using the ConWep module implemented in Abaqus, described in Chapter 2.1.5. These two methods of applying the load were then compared to each other.

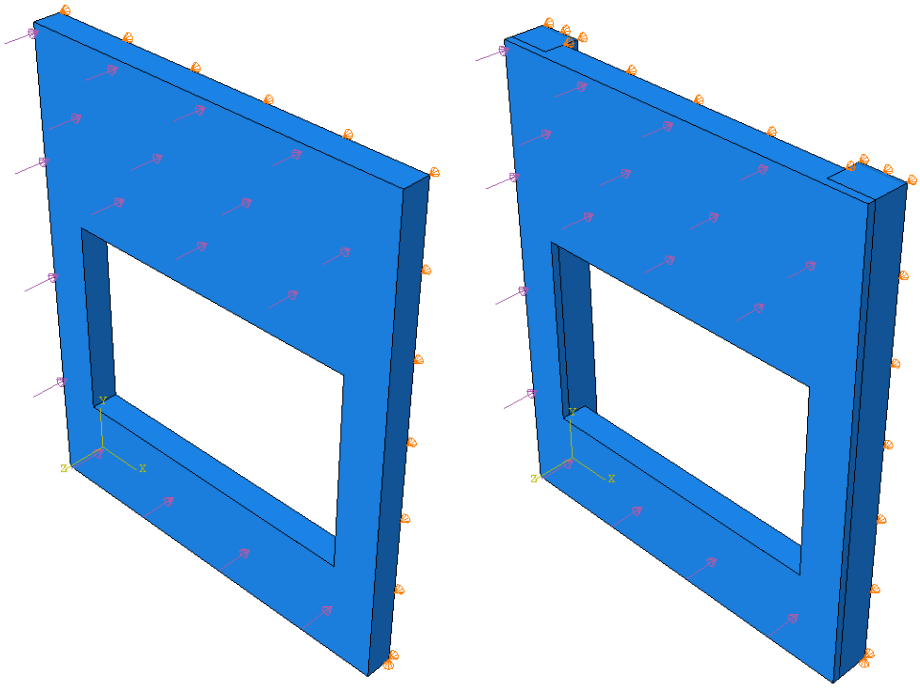

(a) Load on the plate–wall element **(b)** Load on the column–wall element

Figure 3.8: Loads affecting the sandwich elements

Table 3.1: Dynamic blast load parameters for the pressure load

Time [ms]	Load [kPa]
0	420
6.16	0

3.6 Mesh

For the explicit model, the mesh type used for the shell elements was S4R, which is a 4-node doubly curved shell with reduced integration, hourglass control and finite membrane strains. For the solid elements, type C3D8R was used. This is a type of 8-node linear brick, with reduced integration and hourglass control. For the reinforcement in the column, truss element of type T3D2 were used, which are 2-node linear 3D trusses. For the acoustic elements, type AC3D8R was used. These are 8-node linear acoustic bricks, also with reduced integration and hourglass control [19].

The mesh convergence analysis was conducted for the plate–wall element for a time duration of 0.20 s. To check the convergence, the maximal displacement in the z-direction of the inner and outer slabs were noted. Then the error of the various mesh sizes were calculated by comparing them to the result of the analysis with the smallest element sizes. In Figure 3.9, the result is shown. Along with the errors of the different element sizes, the CPU time is plotted.

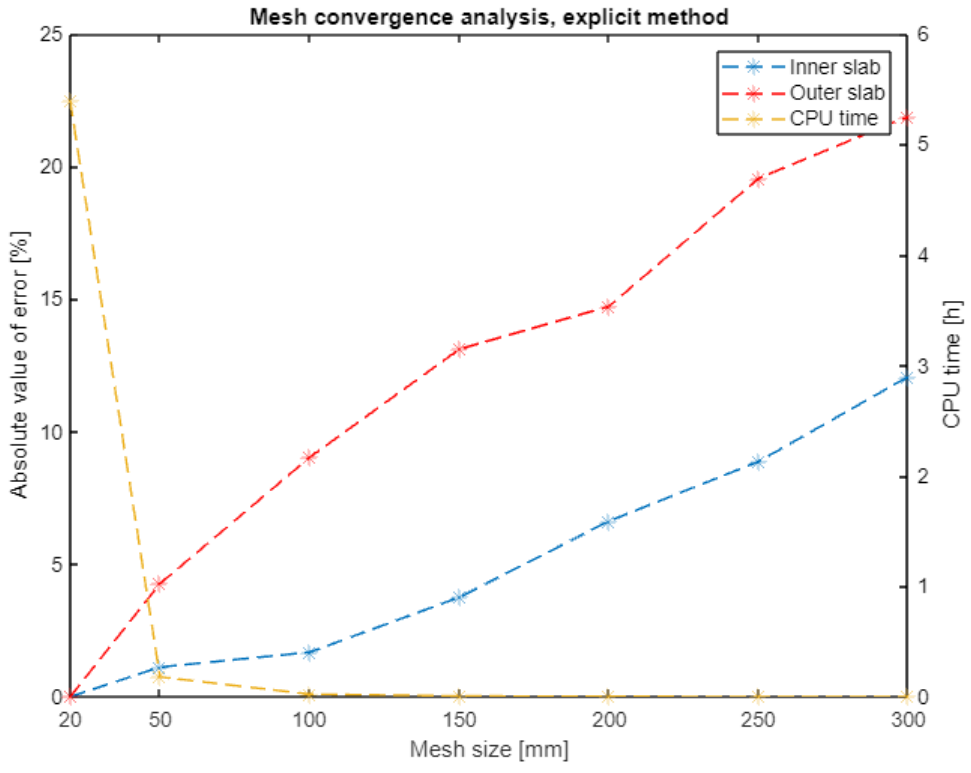

Figure 3.9: Mesh convergence analysis, explicit method

It can be seen that the result starts to diverge instantly when the element size is increased. It can also be observed that the CPU time increased a great extent when the element size was chosen to be 20 mm. Thus, it was chosen to move forward with an element size of 50 mm for the explicit analysis.

It should also be noted that when the element sizes are made smaller, the time step is also made smaller, since this is determined for the smallest element in the model [8]. The time increments were determined automatically.

4 Blast Effects on Wall Elements

In this chapter, the results of the performed analyses are presented. The different designs of the sandwich elements were evaluated and compared using different parameters. These parameters are presented below.

- Energy metrics, see Chapter 4.1.
- Displacement of the inner- and outer slabs, see Chapter 4.2.
- Tensile damage of the concrete, see Chapter 4.3.
- How large of a reaction force that is transferred into the rest of the building, see Chapter 4.4.
- Stress and strain of the reinforcement, see Chapter 4.5.

4.1 Energy Metrics

In Figure 4.1, an example of how the energy should behave is shown. In this figure, it can be observed that the energies that diverge from around zero are the external work, the internal- and kinetic energy, as well as the plastic dissipation- and strain energy. The "artificial" energies, meaning, the artificial strain-, constraint penalty-, penalty contact-, and viscous dissipation energy are all small in comparison.

In Figure 4.2, an example of how the energy should not behave is shown. In this figure, it can be observed that the strain energy goes towards a large negative value, and the plastic- and viscous dissipation energies are becoming larger than the external energy, while the internal energy is becoming negative.

For most models, the energies behaved as they should. However, there were two that acted alike Figure 4.2. In Table 4.1, which energies were stable 0.10 s after the blast hit the outer slab are presented. The selection was made according to the criteria presented in Chapter 2.3.

To compare how the core material affected the energy, the plate–wall element with MSB load was chosen to represent the results. Choosing one geometry, this means that the only differing parameter is the core material. For this, the total internal- and external energies were extracted and compared. The total internal energy is a summation of the strain-, plastic dissipation-, artificial strain-, viscous dissipation-, frictional- and kinetic energy, and the total external energy is a sum of the external work, the contact penalty- and constraint penalty energy [23]. In Figure 4.3, the energies for the models of PF materials of different stiffnesses are compared to the energies from the analysis of the solid slab.

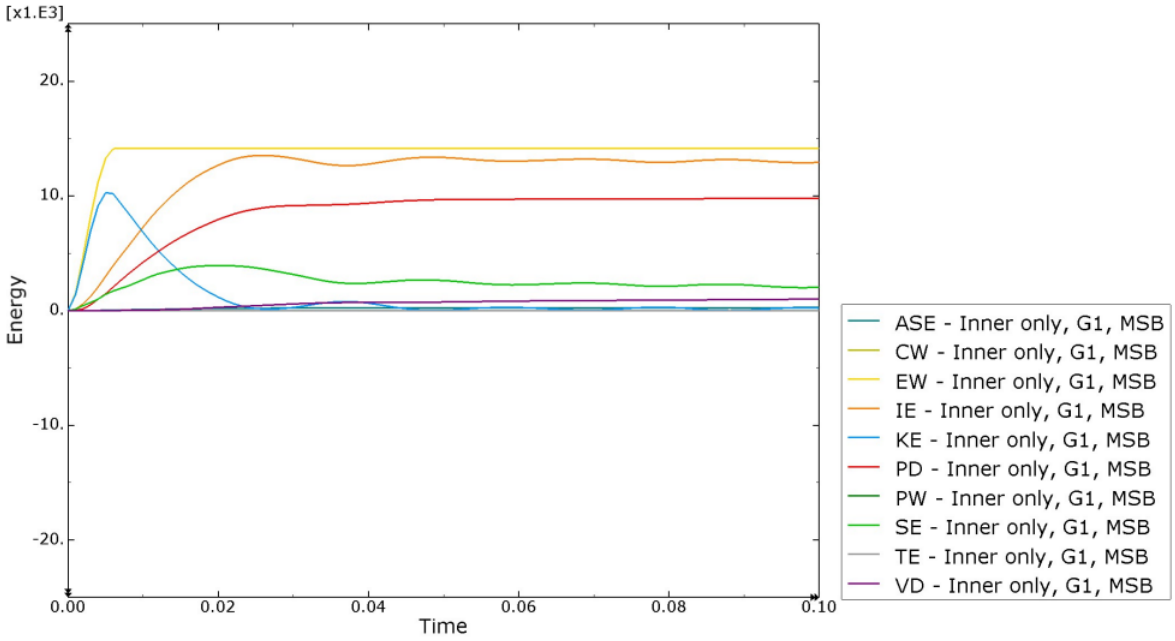

Figure 4.1: Example of how the energy metrics should behave (ASE=Artificial strain energy, CW=Constraint penalty, EW=External work, IE=Internal energy, KE=Kinetic energy, PD=Plastic dissipation, PW=Penalty contact, SE=Strain energy, TE=Total energy and VD=Viscous dissipation). This is shown for the plate–wall element loaded with the MSB load

It can be noted that the internal- and external energies of the four models correspond quite well, meaning that the variation of the total energy is small. It can be observed that the energy level is the lowest for the model where phenolic foam with stiffness 27

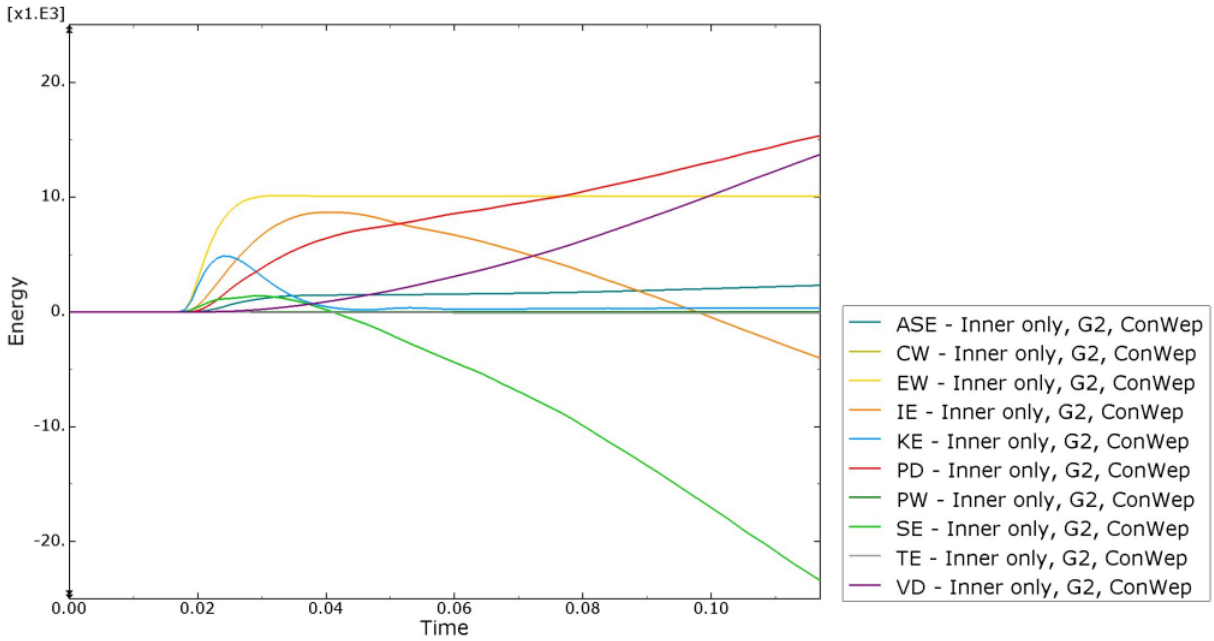

Figure 4.2: Example of how the energy metrics should not vary with time. The energy notations used in this figure are defined in Figure 4.1. This is shown for the column–wall element loaded with the ConWep load

Table 4.1: Compilation of how the energies behaved 0.10 s after the load was applied

Model	MSB		ConWep	
	G1	G2	G1	G2
Inner only	OK	-	OK	-
PF, $E = 27$ MPa	OK	OK	OK	OK
PF, $E = 2.7$ MPa	OK	OK	OK	OK
PF, $E = 0.27$ MPa	OK	OK	OK	OK
Empty	OK	OK	OK	OK
Fluid cavity	OK	OK	OK	OK
Acoustic	OK	OK	OK	OK

MPa is the core material. The energies of the model with only one wall are slightly higher. For the models with phenolic foam with stiffnesses 2.7 and 0.27 MPa as core material, the energies are at a higher level, where the model with stiffness 0.27 MPa is the highest.

The three different ways to model air were also compared in this way, as can be seen in Figure 4.4. From this, it can be noted that the internal- and external energies correspond well. It can also be noted that the models with the fluid cavity and the empty cavity have equal energies during the analysis time. The model with acoustic elements acts the same initially, before the energy reduces, and starts to fluctuate.

Lastly, the models with the highest energy of each category were compared to each other. This means the fluid cavity, PF with a stiffness of 0.27 MPa and the model

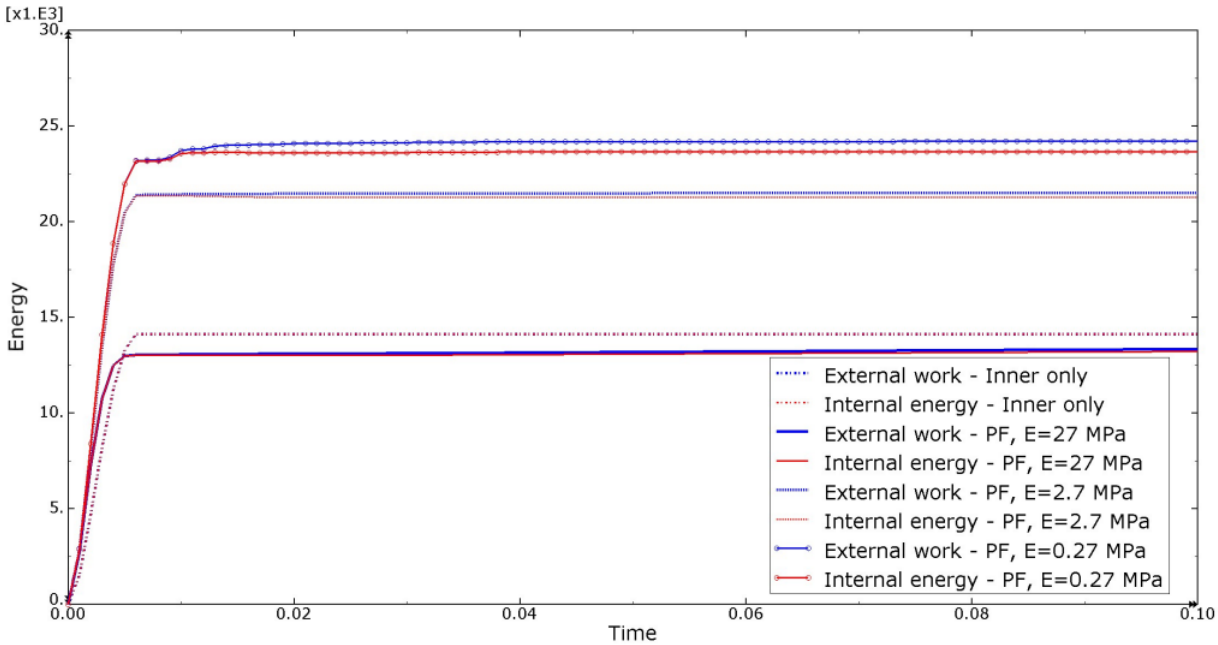

Figure 4.3: Total internal- and external energies for the models with the different PF materials compared to the solid slab, shown for the plate–wall element loaded with MSB load

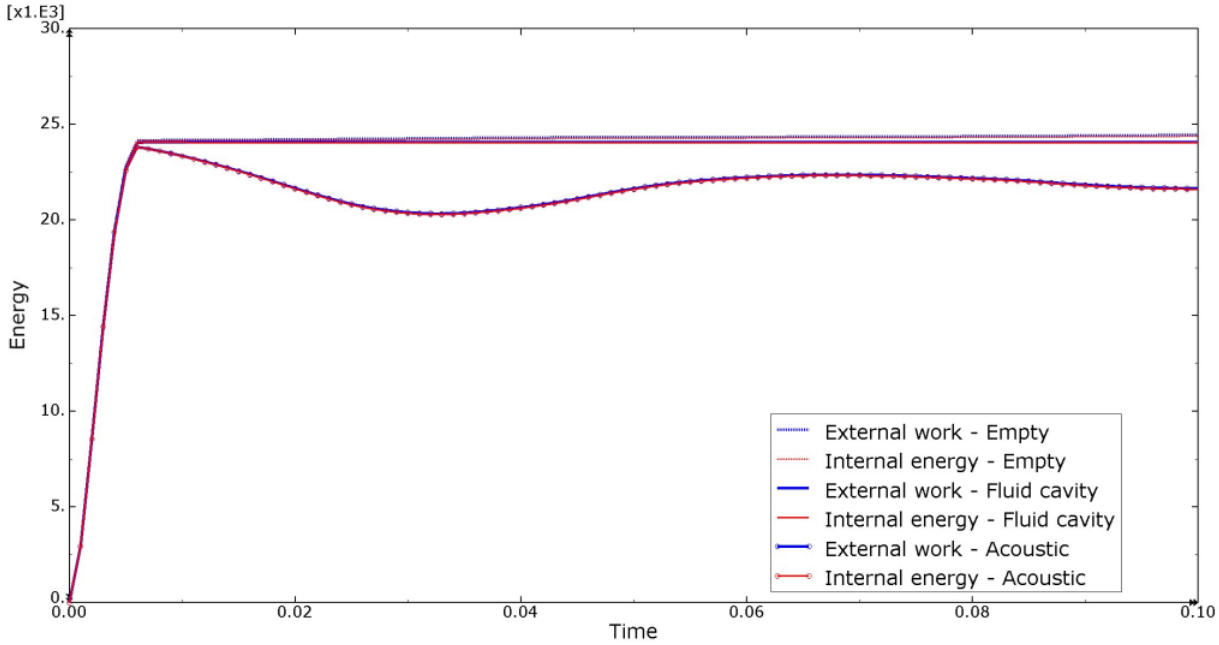

Figure 4.4: Total internal- and external energies for the different air models, shown for the plate–wall element loaded with MSB load

with a solid slab. This is shown in Figure 4.5. With this figure, it can be observed that the lowest energy levels are reached when the wall consists of a solid slab. It can also be noted that the energies of the design with air compared to phenolic foam with a stiffness of 0.27 MPa, shows that these reach almost the same level.

How the energy absorption varied with the foam stiffness was also investigated more

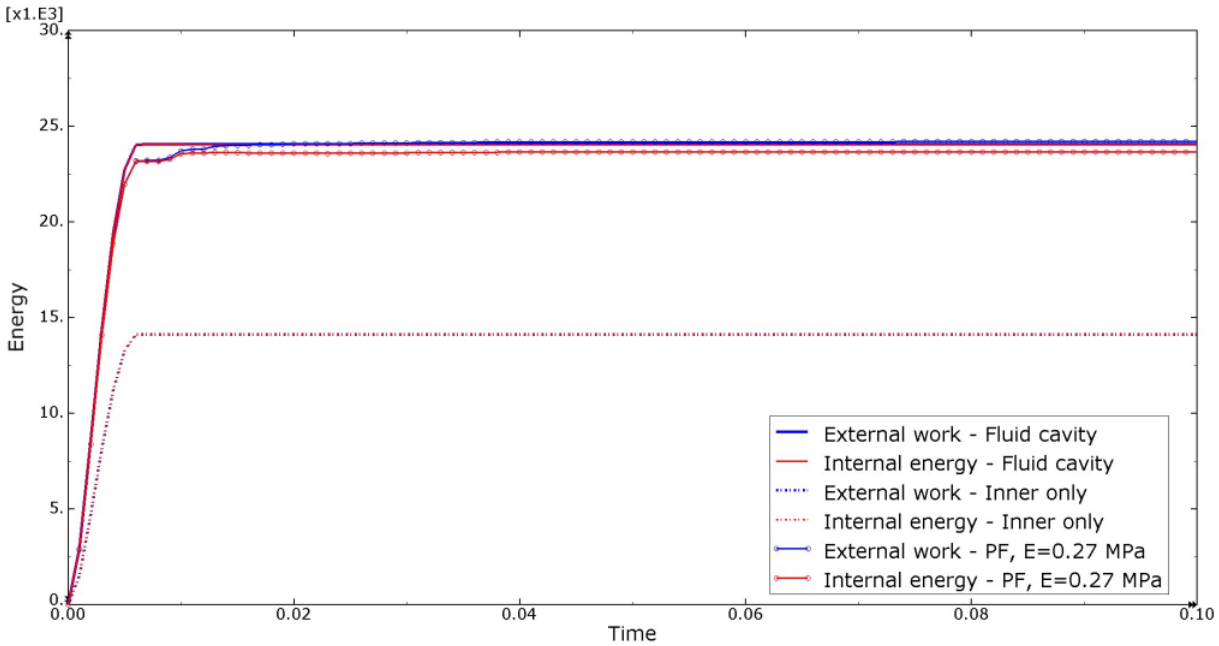

Figure 4.5: Total internal- and external energies for the fluid cavity, PF with a stiffness of 0.27 MPa and the solid slab, shown for the plate–wall element loaded with MSB load

in depth. This is shown in Figure 4.6, in which the left subfigure shows the actual values, and the right shows at which percentage of the highest energy – i.e. from the foam with stiffness 0.27 MPa – that the foams of other stiffnesses reach. In this figure, it can be observed that the levels of the energies are different dependant on how the load is applied. It can be noted, however, that the variations among the models of the same load application are similar. In the right figure, the variation of the percentage can be observed. This shows that the variations have similar progress, with a noted reduction between 11% and 22% for a stiffness of 2.7 MPa, and between 44% and 62% for a stiffness of 27 MPa.

4.2 Displacement

Another relevant result to observe are the displacements the slabs get from the blast. In this section, the displacements of the inner- and outer slabs will be compared for the different models. This will be done for a duration of 0.10 s.

4.2.1 MSB Load

In Figure 4.7, the maximal displacements of the inner wall for the models with phenolic foam are compiled with the model of the solid wall. These are shown for both concrete geometries. This figure shows that – for both wall geometries – the deflection of the solid wall is the largest, followed by the model with foam of stiffness 2.7 MPa, the foam of stiffness 27 MPa, and the smallest deflection for the foam of stiffness 0.27 MPa.

In Figure 4.8, the maximal displacements for the outer wall for the models with phenolic foam as core material are shown. These are shown for both the plate- and column–wall element. From this figure, it can be observed that the largest displacement is reached when the stiffness of the foam is lower. If the stiffness is 27 or 2.7 MPa leads

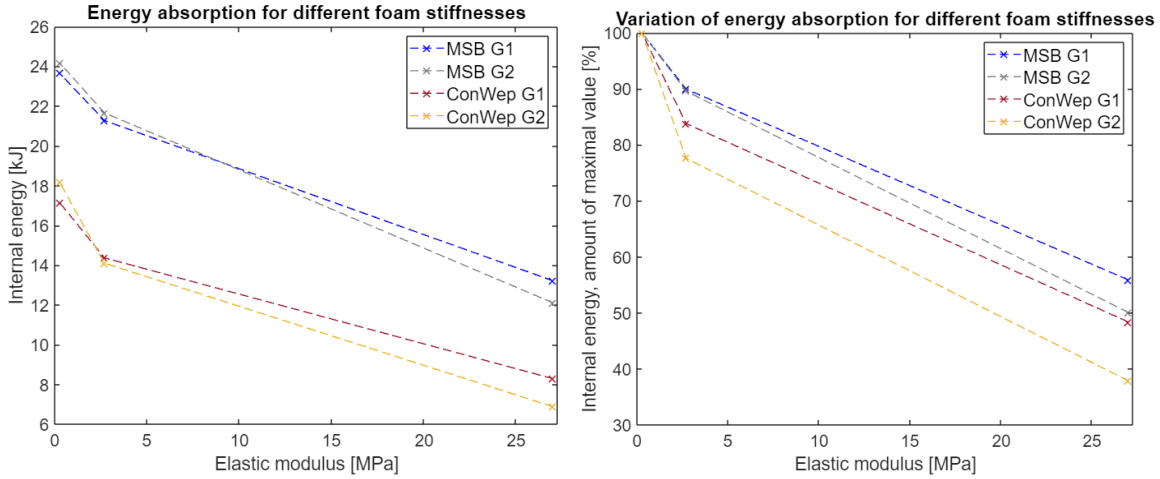

(a) Energy variation **(b)** Percentage of energy variation

Figure 4.6: Variation of energy with the different foam stiffnesses, shown for both of the load application methods as well as geometries

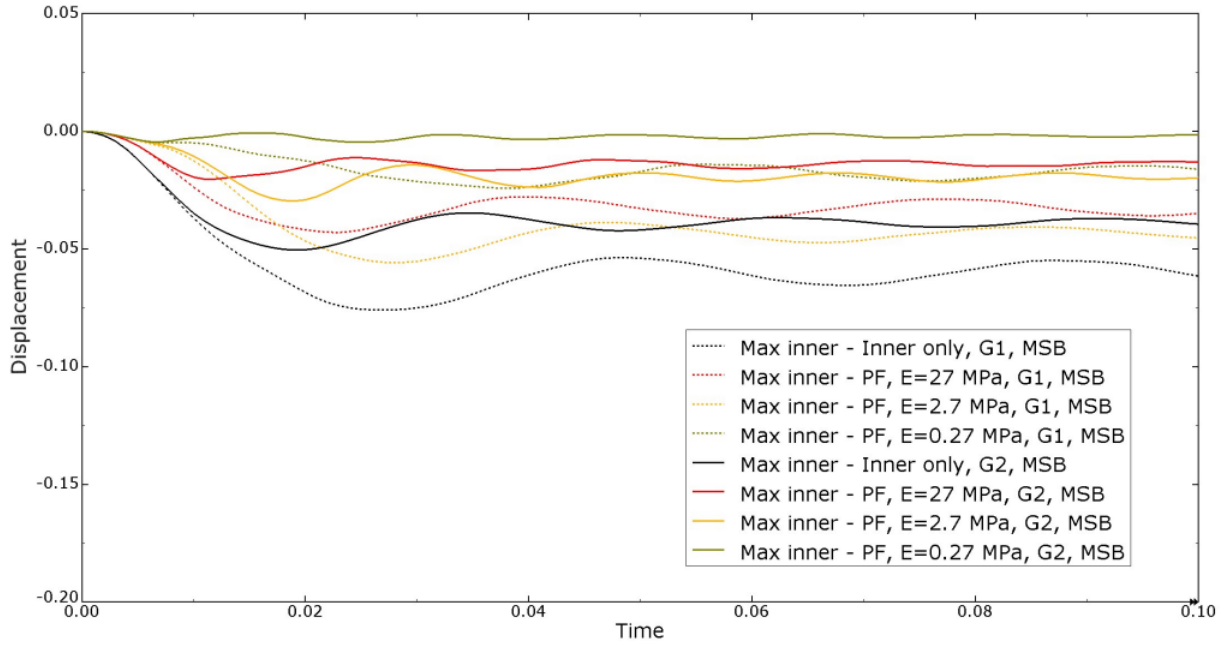

Figure 4.7: Displacement for the inner slab for the models with phenolic foam compared to the solid slab, shown for the plate- and column–wall element with the MSB load

to no significant difference.

In Figure 4.9, the maximal displacement for the inner slab when the core consists of air modelled in three different ways is shown, for both the concrete geometries. As can be observed from this figure, the displacements of the different air models – and both wall geometries – are equal to each other, and all are around zero.

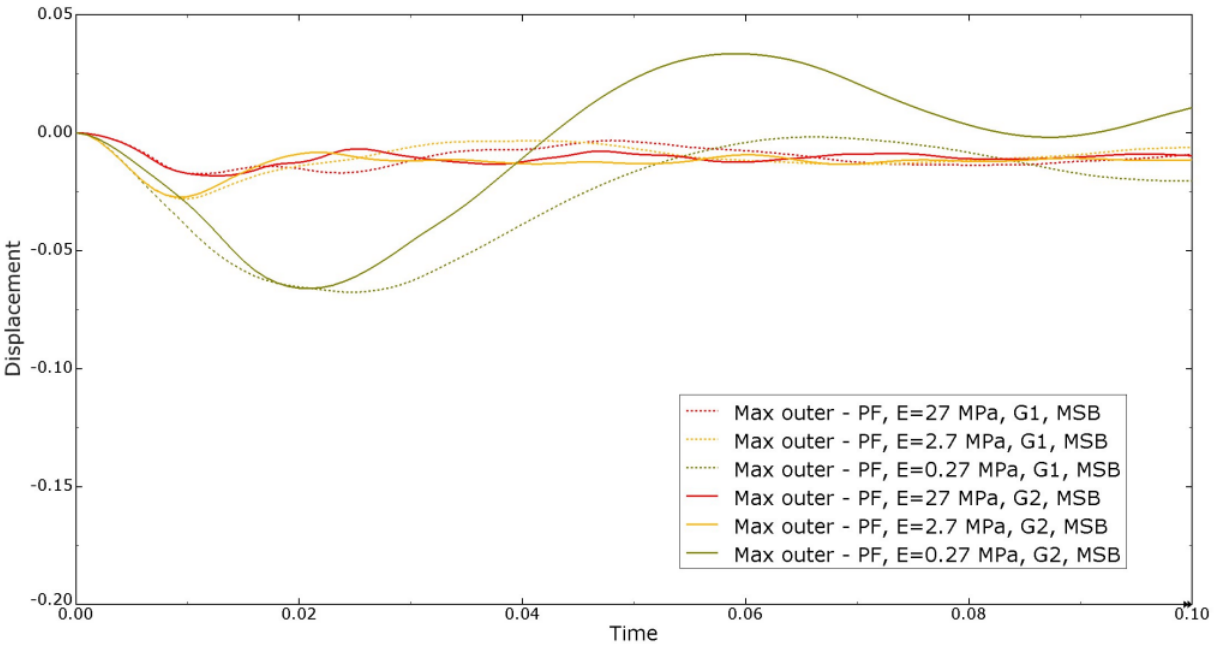

Figure 4.8: Displacement for the outer slab for the models with phenolic foam, shown for the plate- and column–wall element with the MSB load

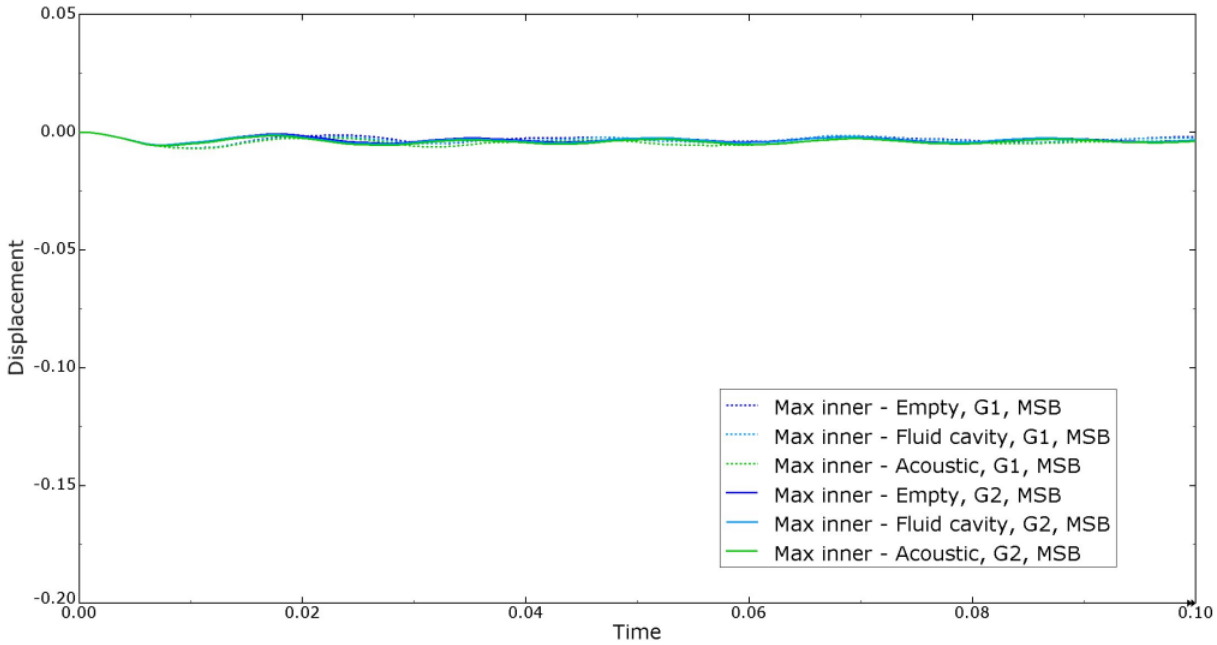

Figure 4.9: Displacement for the inner slab for the various models of air, shown for the plate- and column–wall element with the MSB load

In Figure 4.10, the maximal displacements of the outer walls are shown for the air models. As can be observed, the displacements vary some between the models. The largest displacement shows for the model with the empty cavity, both for the plate- and column–wall element. The models with a fluid cavity and acoustic elements show more similar displacements, with the acoustic elements leading to the smallest result. For the models with the empty cavity, as well as for the fluid cavity model, the column–wall element leads to the largest displacements, while it for the model with acoustic

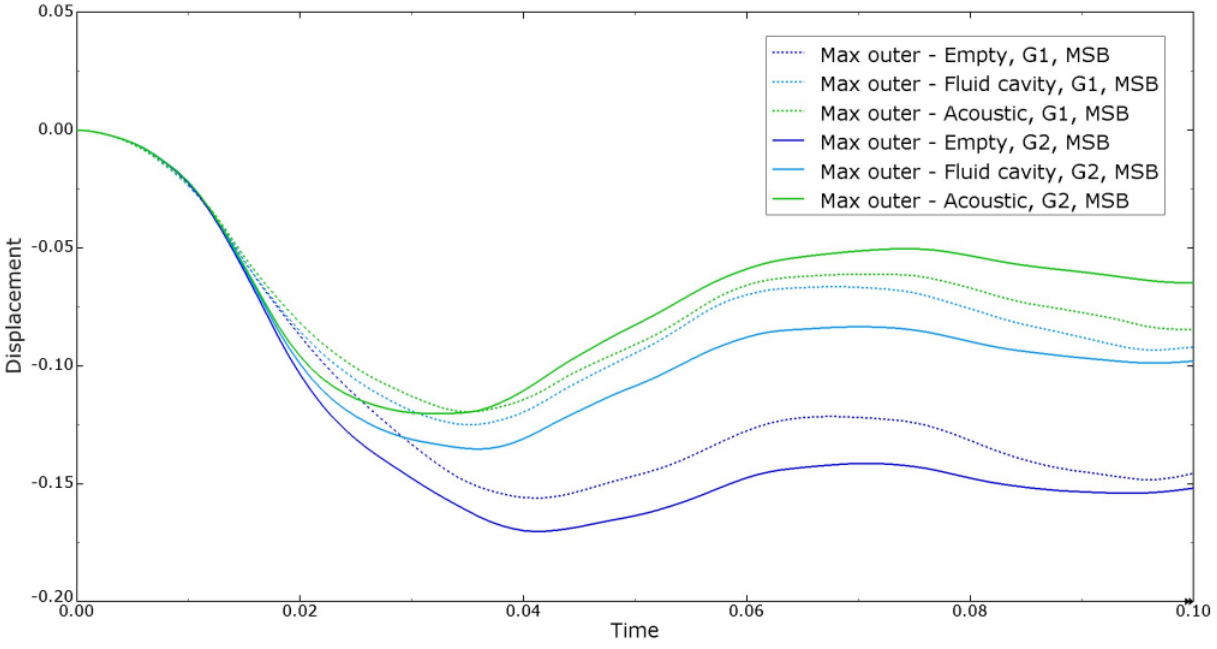

Figure 4.10: Displacement for the outer slab for the various models of air, shown for the plate- and column–wall element with the MSB load

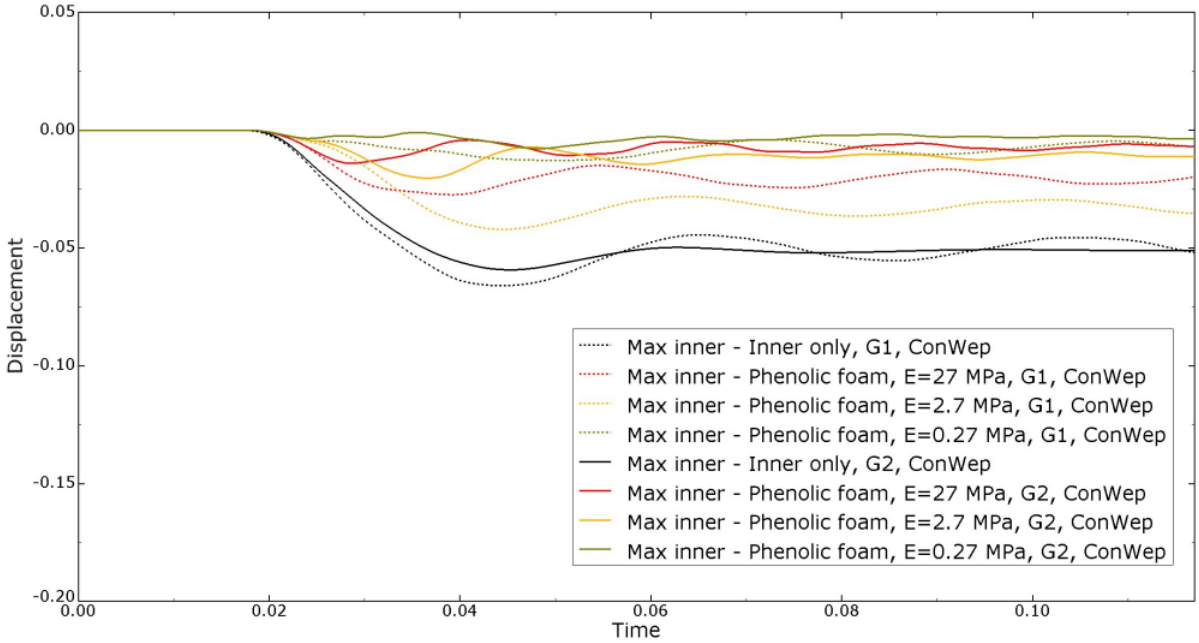

Figure 4.11: Displacement for the inner slab for the models with phenolic foam compared to the solid slab, shown for the plate- and column–wall element with the MSB load

elements is the plate–wall element that shows the largest displacements.

4.2.2 ConWep Load

In Figure 4.11, the maximal displacement of the inner wall from the models with phenolic foam as core are compared to the model with a solid wall. This is shown both for the plate- and the column–wall element. From the figure, it can be observed that the solid wall gets the largest deflections, both for the plate- and column–wall element. This is followed by the foam of stiffness 2.7 MPa, and then by the foam of stiffness 27 MPa. The smallest displacements are gained when the foam has the stiffness 0.27 MPa. The order is the same for both geometries.

In Figure 4.12, the maximal outer wall displacement is shown for the models with phenolic foam cores. In this figure, it can be observed that the displacement is the largest when the stiffness of the foam is lower. There is no large difference between if the stiffness is 27 or 2.7 MPa. It can also be noted that the sizes of the displacements show little variation between the two geometries.

Figure 4.13 shows the deflection of the inner slab when the core consists of air modelled in the three different ways. In this figure, it can be observed that the displacements are all around zero no matter which geometry or way of modelling the core that is used.

In Figure 4.14, the displacements for the outer wall of the model where the core consists of air is shown. In this figure, it can be observed that the displacement is the largest for the model with the empty cavity. For the models with a fluid cavity and acoustic

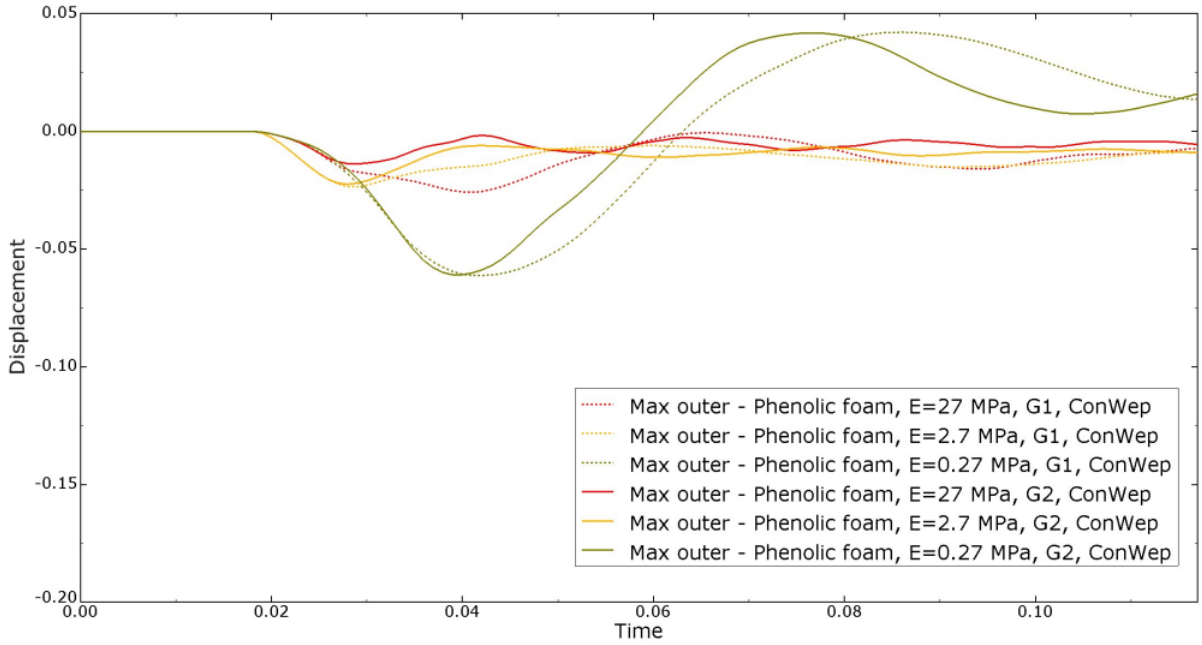

Figure 4.12: Displacement for the outer slab for the models with phenolic foam, shown for the plate- and column–wall element with the ConWep load

elements, the displacements are more equal, with the acoustic elements leading to the smallest deflections. As for the MSB loaded walls, the column–wall elements show the largest displacements for the models with the empty cavity, as for the fluid cavity. For the model with acoustic elements it is the opposite way, where the plate–wall element gains the largest displacements.

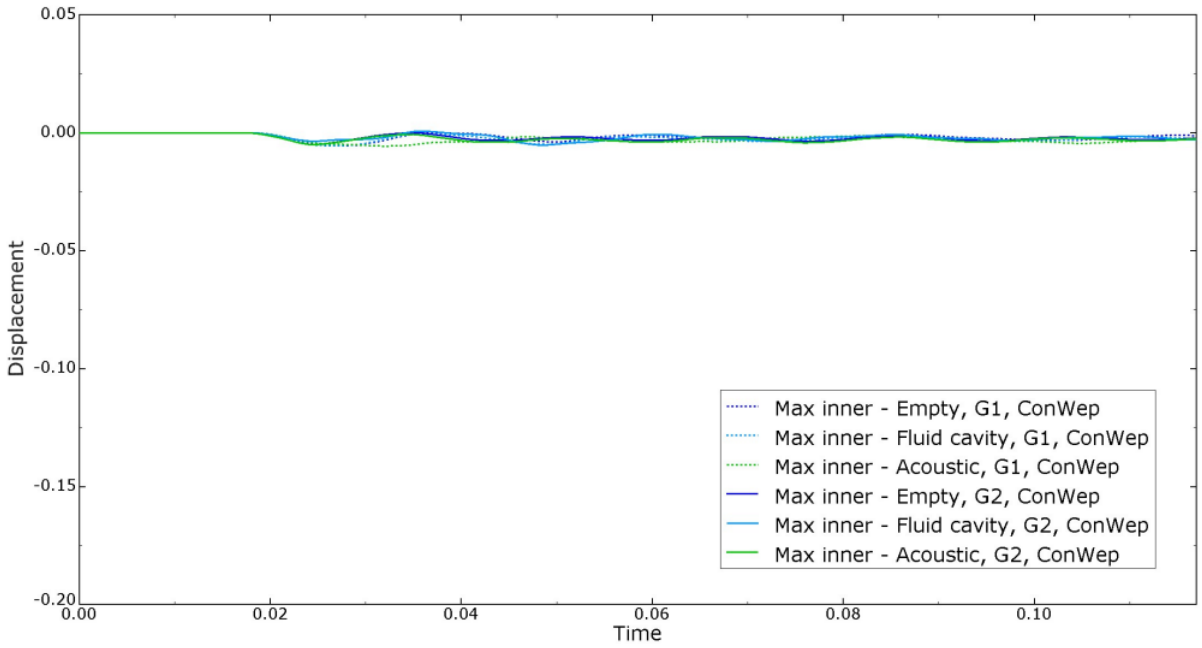

Figure 4.13: Displacement for the inner slab for the models with air, shown for the plate- and column–wall element with the ConWep load

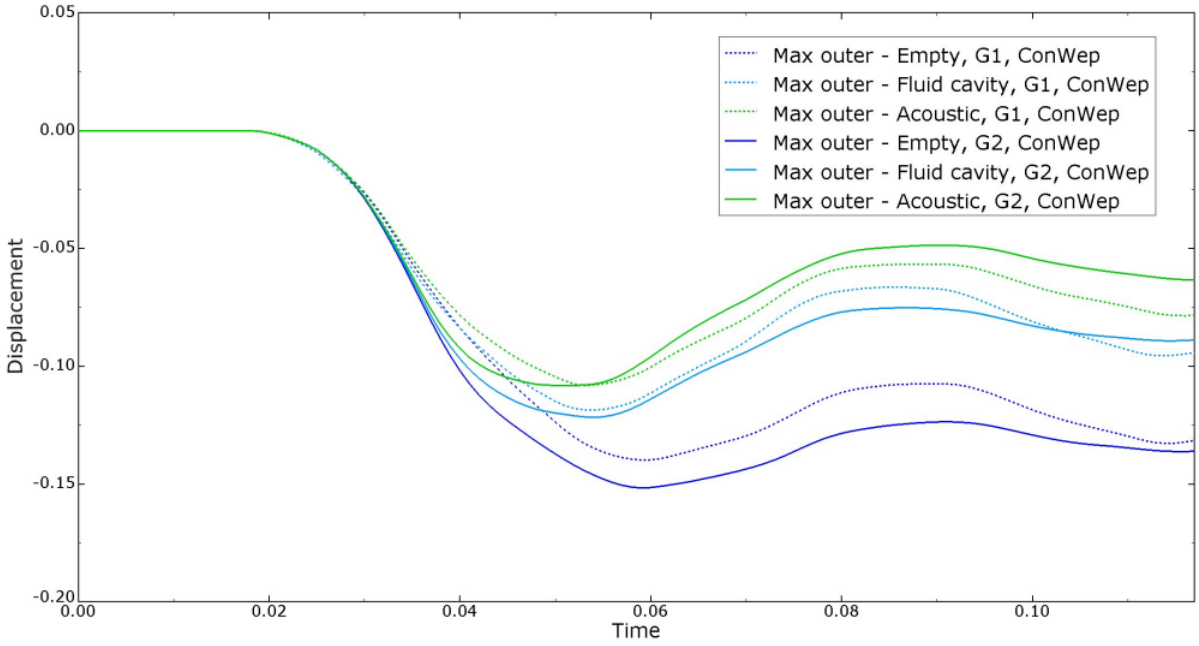

Figure 4.14: Displacement for the outer slab for the models with air, shown for the plate- and column–wall element with the ConWep load

4.3 Tensile Damage

When subjected to the blast, parts of the concrete wall will crack and fail. Most of the damage to the concrete will be tensile in nature. In this section, the damage that the concrete accumulates due to the blast will be presented. This will be done 0.10 s after the load acts. For showing the results, the models affected by the MSB load were chosen. For the visualisation of the result, red means full damage, and blue means no damage.

4.3.1 Plate–Wall Element

In Figure 4.15, the tensile damage accumulated by the solid wall is shown. From this figure, it can be observed that the back of the wall is almost completely damaged. The front of the wall is fully damaged in the corners, with cracks going in towards the middle of the window.

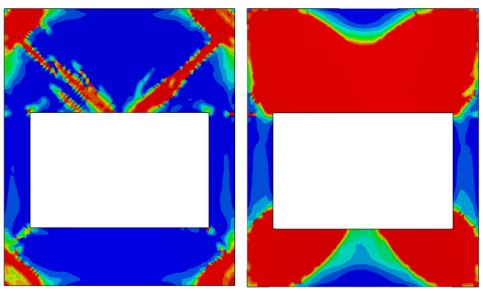

(a) Inner front **(b)** Inner back

Figure 4.15: Damage for the plate–wall element, solid wall, shown for the MSB load

In Figure 4.16, the damage for the outer- and inner slab of the model with phenolic foam of stiffness 27 MPa as core material is shown. From this result, it can be observed that the back of the inner wall gets damaged mostly everywhere, with the front showing large cracks. The back of the outer slab shows some damage almost everywhere, but the damage is not fully developed aside from some parts above and below the window. The front of the outer slab has most damage above and below the window as well.

In Figure 4.17, the damage for the outer- and inner wall for the model with phenolic foam with stiffness 2.7 MPa is shown. It can be observed that the inner wall is completely damaged in a cross shape at the back, with prominent cracks showing in the front. The outer slab shows considerable damage both at the back and at the front, with many cracks showing in the front.

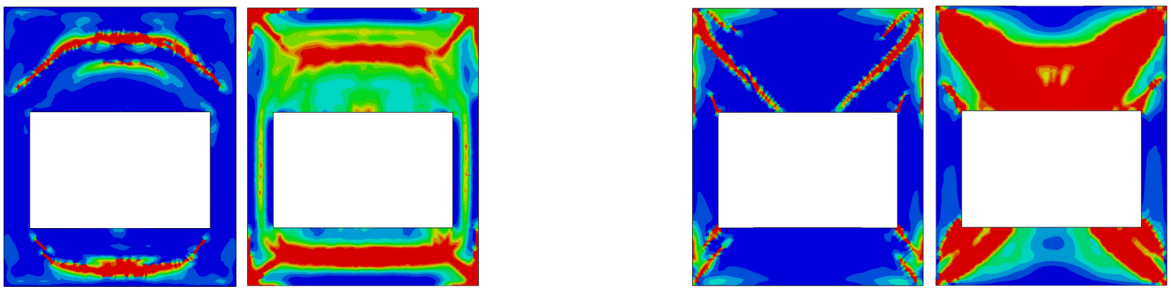

(a) Outer front **(b)** Outer back **(c)** Inner front **(d)** Inner back

Figure 4.16: Damage for the plate–wall element, phenolic foam with E=27 MPa, shown for the MSB load

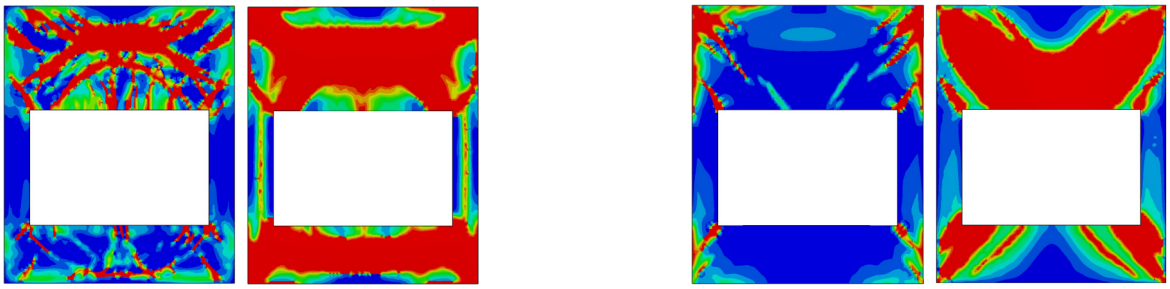

(a) Outer front **(b)** Outer back **(c)** Inner front **(d)** Inner back

Figure 4.17: Damage for the plate–wall element, phenolic foam with E=2.7 MPa, shown for the MSB load

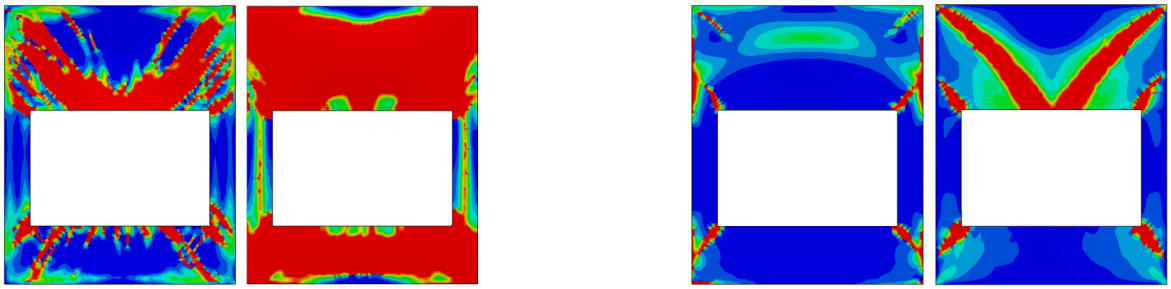

(a) Outer front **(b)** Outer back **(c)** Inner front **(d)** Inner back

Figure 4.18: Damage for the plate–wall element, phenolic foam with E=0.27 MPa, shown for the MSB load

In Figure 4.18, the damage for the model with phenolic foam of stiffness 0.27 MPa is shown. This foam core shows less damage to the inner slab, with the largest damage showing in a cross shape at the top, as well as from the corners of the windows. The front of the inner slab has the most damage showing at the corner of the windows. The back of the outer slab is almost fully damaged, while the front shows the damage in a cross shape, with distinct cracks.

In Figures 4.19–4.21, the damage of the outer- and inner wall with air modelled in different ways are shown. Figure 4.19 shows the model with the fluid cavity, Figure 4.20 shows the model with the acoustic elements, and Figure 4.21 with the empty cavity. The different ways of modelling the air results in similar damage to the concrete. The inner walls are mostly damaged around the corners of the window openings, with some damage around the middle of the top part at the front. The outer wall is at full damage for almost the whole backside, while the front part mostly is damaged around the window openings, as well as with some cracks along the boundary.

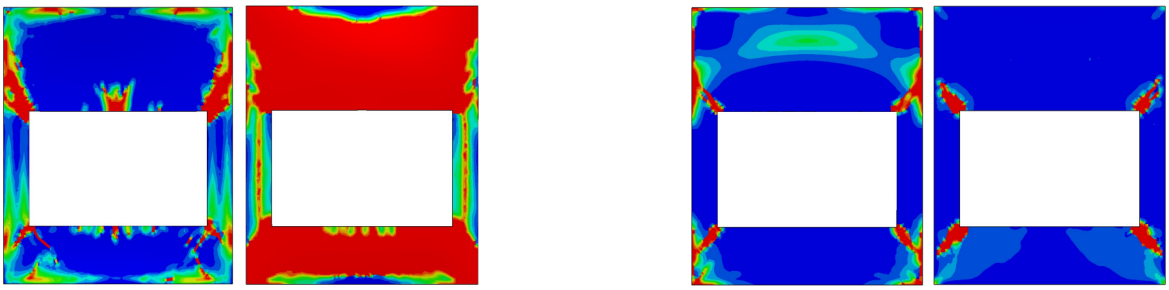

(a) Outer front **(b)** Outer back **(c)** Inner front **(d)** Inner back

Figure 4.19: Damage for the plate–wall element, fluid cavity, shown for the MSB load

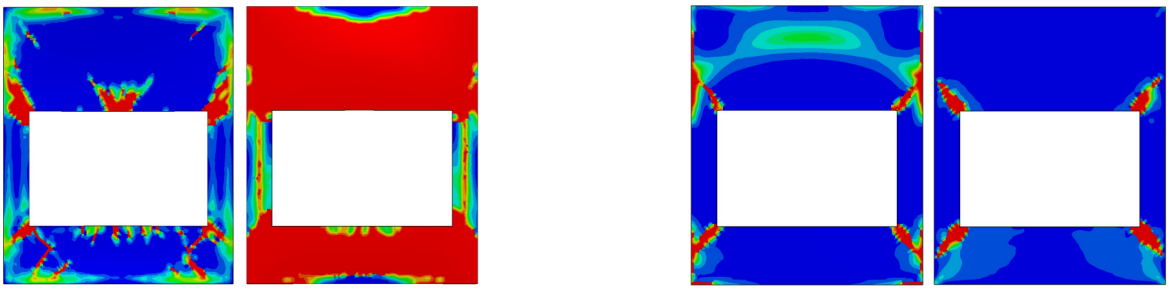

(a) Outer front **(b)** Outer back **(c)** Inner front **(d)** Inner back

Figure 4.20: Damage for the plate–wall element, acoustic, shown for the MSB load

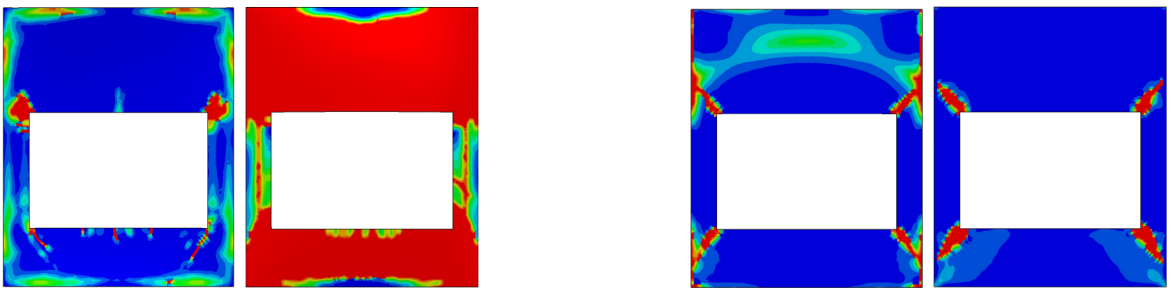

(a) Outer front **(b)** Outer back **(c)** Inner front **(d)** Inner back

Figure 4.21: Damage for the plate–wall element, empty, shown for the MSB load

4.3.2 Column–Wall Element

In Figure 4.22, the damage of the inner slab is shown for the non-sandwich wall. From the figure, it can be observed that the columns accumulates quite a lot of damage. The back part of the slab gets fully damaged in a cross shape, with some damage showing over the whole section. The front of the slab gets some damage at the section where this is connected to the column, as well as some cracks in toward the middle.

In Figure 4.23, the damage of the outer- and inner walls are shown for the model with phenolic foam of stiffness 27 MPa. From this figure, it can be observed that the columns get some damage around the boundary, as well as around the bottom part of the window corners. The back of the inner slab gets completely damaged in a cross pattern, with some damage over the whole surface. The front of the inner slab gets some damage around the line where the slab is connected to the column, with some additional cracks. The whole back of the outer slab gets some damage, with the worst occurring above and underneath the window. The front of the outer slab gets damaged in a circular crack pattern, connected to the window opening.

In Figure 4.24, the damage for the slabs of the model with phenolic foam of stiffness 2.7 MPa is shown. This figure shows that the column gets some damage around the boundary, as well as in connection to the window opening. The back of the inner slab gets damaged almost everywhere, with the worst part being in a cross over the whole part. The front of the inner wall gets damage at the point of connection between the slab and the column, as well as some cracks going towards the window. The back of the outer slab gets damaged over the whole surface, with the worst damage occurring

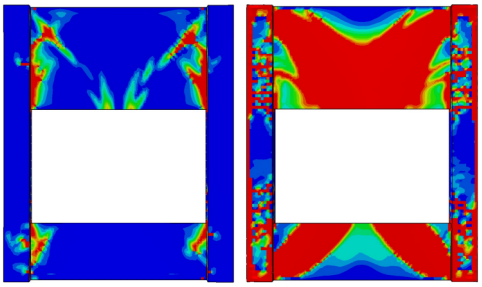

(a) Inner front **(b)** Inner back

Figure 4.22: Damage for the column–wall element, solid wall, shown for the MSB load

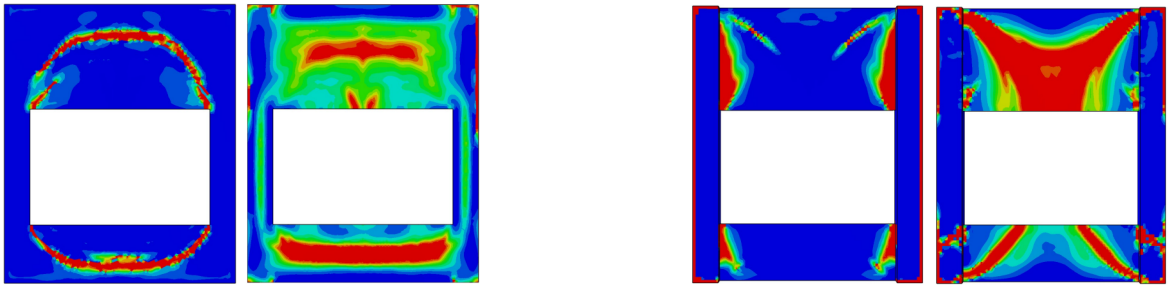

(a) Outer front **(b)** Outer back **(c)** Inner front **(d)** Inner back

Figure 4.23: Damage for the column–wall element, phenolic foam with E=27 MPa, shown for the MSB load

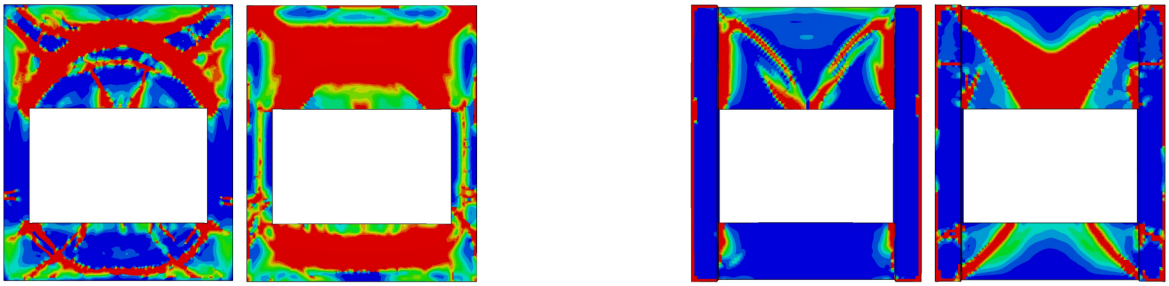

(a) Outer front **(b)** Outer back **(c)** Inner front **(d)** Inner back

Figure 4.24: Damage for the column–wall element, phenolic foam with E=2.7 MPa, shown for the MSB load

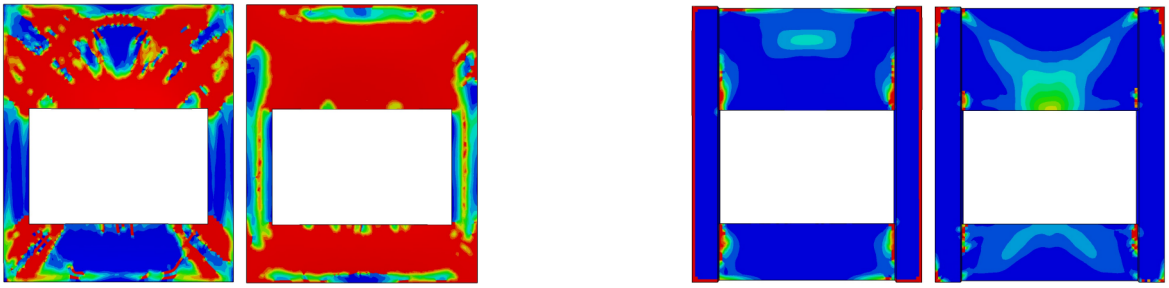

(a) Outer front **(b)** Outer back **(c)** Inner front **(d)** Inner back

Figure 4.25: Damage for the column–wall element, phenolic foam with E=0.27 MPa, shown for the MSB load

as a frame around the window, and up towards the corners. The front of the outer slab gets its worst damage in a circular shape around the window, with cracks also going up towards the corners.

Figure 4.25 shows the damage of the slabs for the model with phenolic foam of a stiffness of 0.27 MPa as a core. With the reduced foam stiffness, the inner slab shows less damage, with the most showing around the boundaries of the column as well as some around the point of connection between the inner slab and the column. The back of the outer slab is almost fully damaged, while the front shows large cracks in a cross pattern.

Figures 4.26–4.28 shows the damage of the outer- and inner slab for the three different air models. Figure 4.26 shows the result for the fluid cavity model, Figure 4.27 shows the result of the model with acoustic elements, and Figure 4.28 shows for the model with the empty cavity. The air models show some damage to the front of the columns around the boundary, with some damage in the middle of the back of the inner slab. For the front of the inner slab, the damage is centered around the connection between the slab and column. The back of the inner slabs get completely damaged, with the front showing a varied amount of cracks, both from the corners of the window, as well as around the boundary.

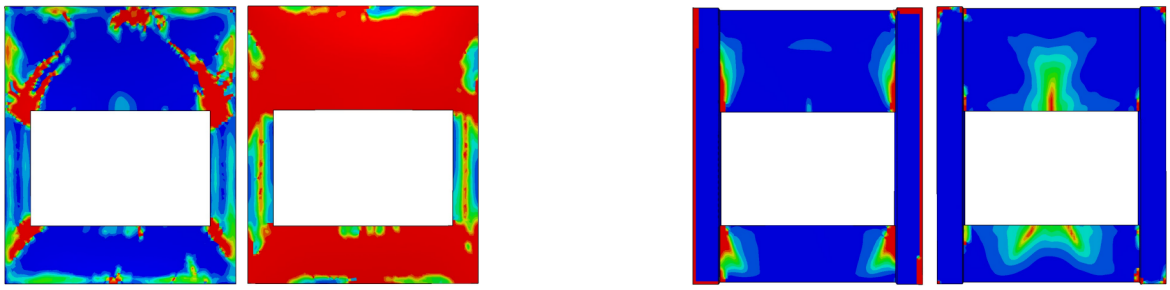

(a) Outer front **(b)** Outer back **(c)** Inner front **(d)** Inner back

Figure 4.26: Damage for the column–wall element, fluid cavity, shown for the MSB load

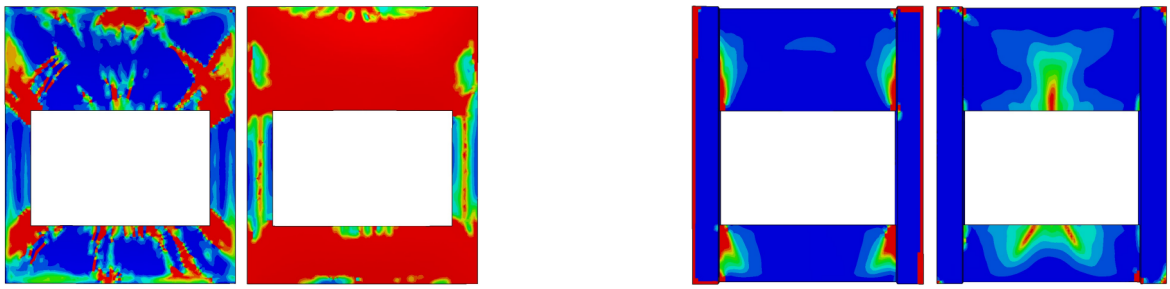

(a) Outer front **(b)** Outer back **(c)** Inner front **(d)** Inner back

Figure 4.27: Damage for the column–wall element, acoustic, shown for the MSB load

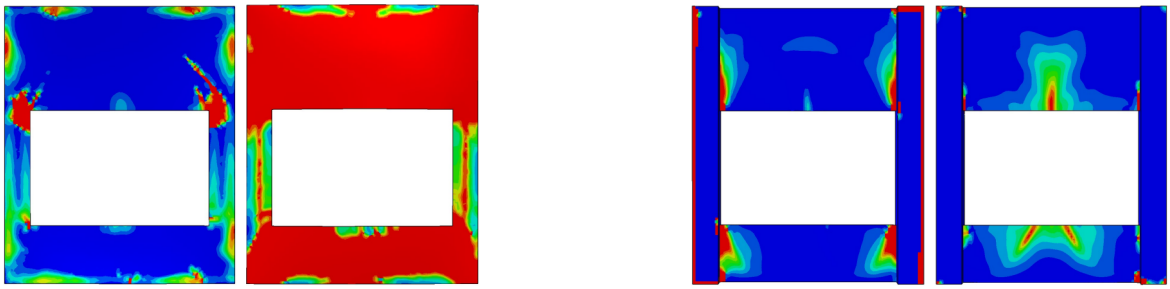

(a) Outer front **(b)** Outer back **(c)** Inner front **(d)** Inner back

Figure 4.28: Damage for the column–wall element, empty, shown for the MSB load

4.4 Reaction Force

Another parameter that can be compared is the total reaction force transferred into the rest of the building. For this, a lesser value means that a larger amount of energy was absorbed by the wall element, which is positive for the structure.

In this section, the reaction forces will be presented for the different designs of the wall. This will be presented for the first 10 ms of the analysis, since the peak occurs during this time period. In the case of the ConWep loading, this is applied after the blast has hit the wall.

4.4.1 MSB Load

In Figure 4.29, a compilation of the reaction forces for the MSB loaded plate–wall element with different core layers are shown. In this figure, it can be observed that the maximal peak of the reaction force for the several models are of a similar size. It can also be noted that for the solid wall, the peak is reached instantly, while it for the sandwich walls takes a longer duration.

In Figure 4.30, the reaction forces of the MSB loaded column–wall element are shown for the different core layers. This figure shows that the reaction force of the solid wall is the highest compared to the others. It also shows that the different air models lead to equal results. The phenolic foams leads to similar results initially, but after a time, the foam of the lowest stiffness shows the smallest reaction force.

For a clear comparison of the reaction force of the two geometries (G1, G2), the results of the plate- and column–wall elements were plotted together. In Figure 4.31, the reaction forces when only the inner parts were modelled are shown. It can be observed that the reaction force for the plate–wall element in the beginning rises with a steeper inclination, and, at once, hits its peak. The reaction force of the column–wall element hits its peak after a slightly longer time, with a slightly lower value.

In Figure 4.32, the reaction forces for the models with phenolic foam as the core material are shown. Comparing the foams and geometries to each other shows that the foams lead to similar reactions in the beginning, with the values deviating some after about 1.5 ms, leading to the stiffer foams having larger reaction forces. It can be observed that use of the plate–wall element leads to larger reaction forces compared to the column–wall element.

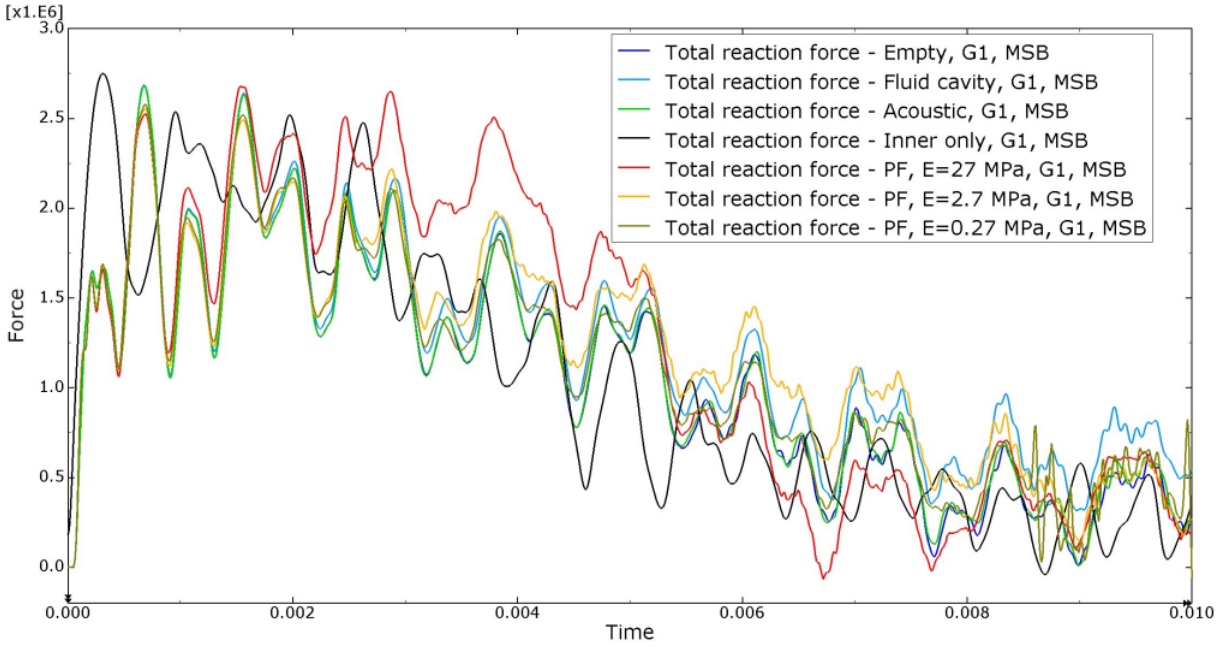

Figure 4.29: Compilation of the reaction forces for all the models of the plate–wall element, shown for the MSB load

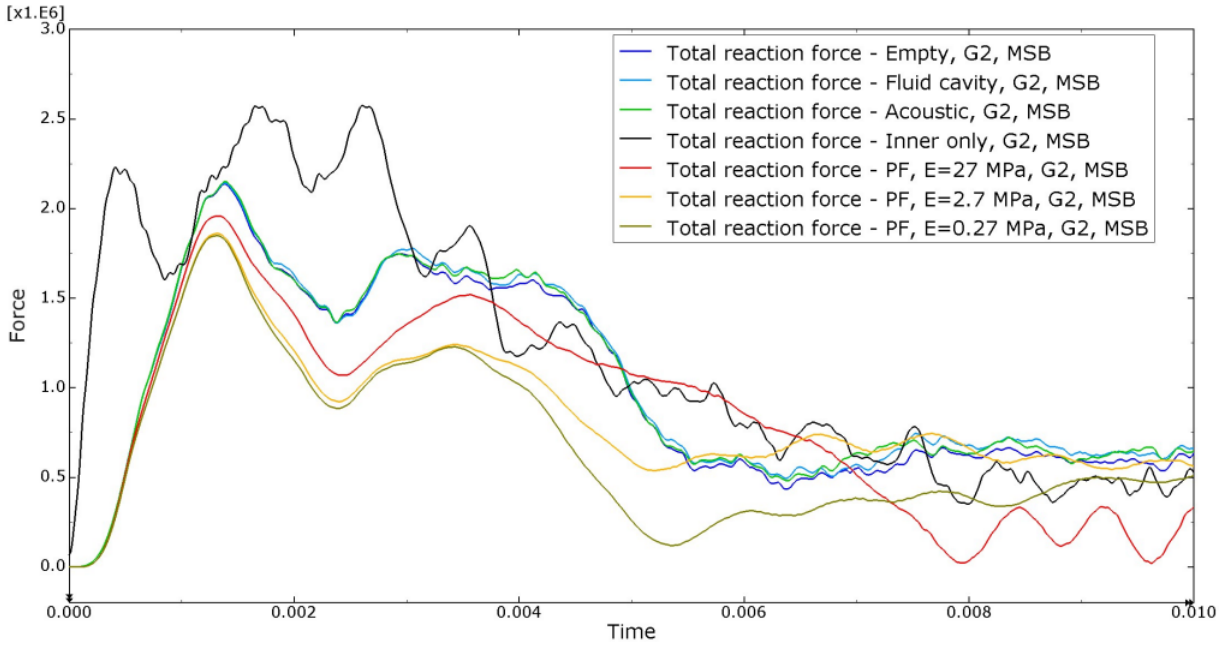

Figure 4.30: Compilation of the reaction forces for all the models of the column–wall element, shown for the MSB load

In Figure 4.33, the reaction forces for the models with air as the core material are shown. Use of the plate–wall element leads to generally larger reaction forces, that occur earlier than for the column–wall element. The reaction forces gained from the different ways of modelling the air correspond well to each other.

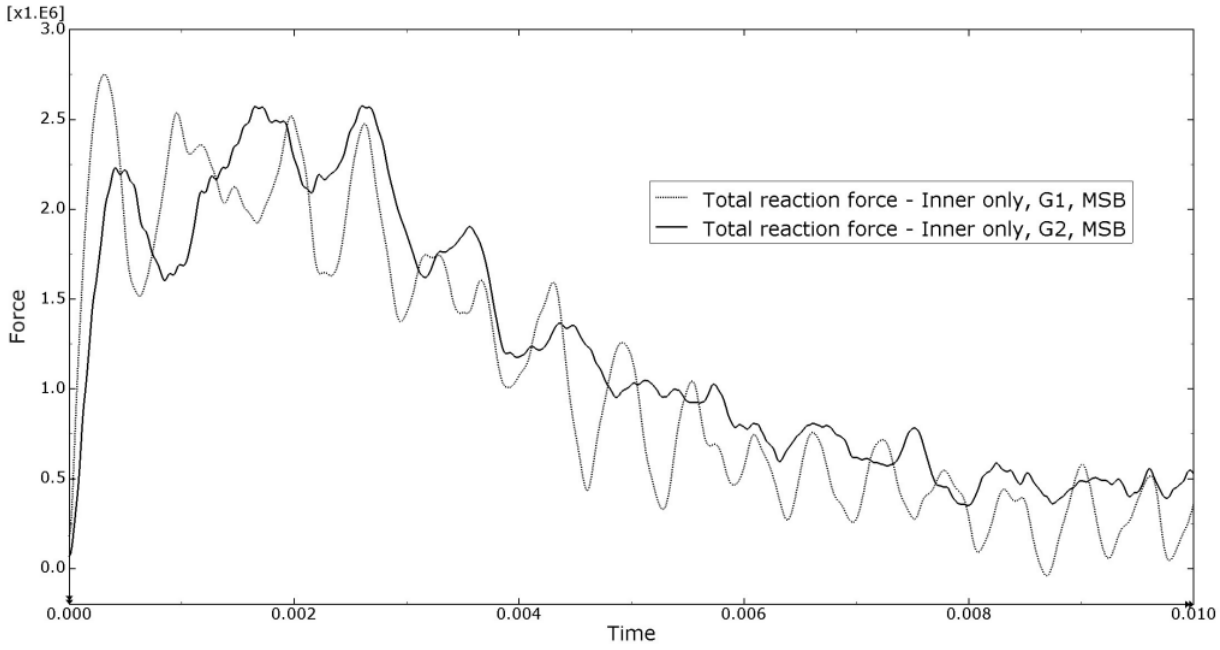

Figure 4.31: Compilation of the reaction forces for the inner slab only, the plate- and column–wall element, shown for the MSB load

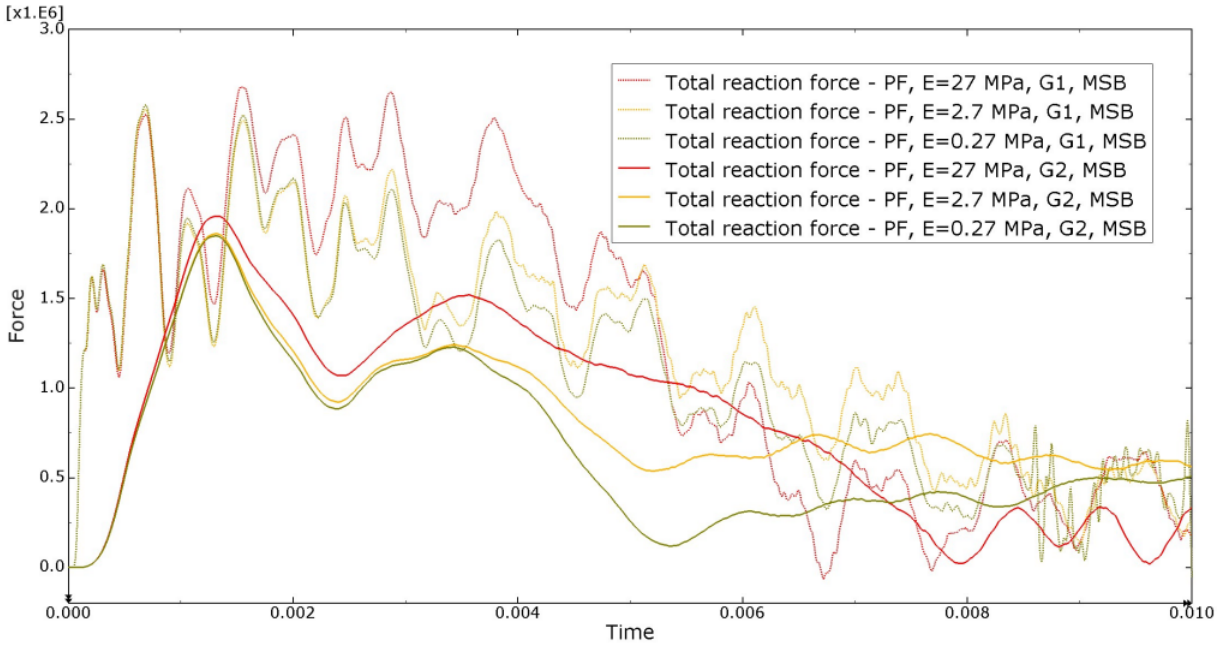

Figure 4.32: Compilation of the reaction forces when the core is made up of phenolic foam of different stiffnesses, for both the plate- and column–wall elements, shown for the MSB load

4.4.2 ConWep Load

In Figure 4.34, a compilation of the reaction forces for the ConWep loaded plate–wall element with different core layers are shown. From this figure, it can be noted that initially, the reaction force is the largest for the solid wall, but at the approximate time 21 ms after the analysis started, the model with the stiffest foam core shows a

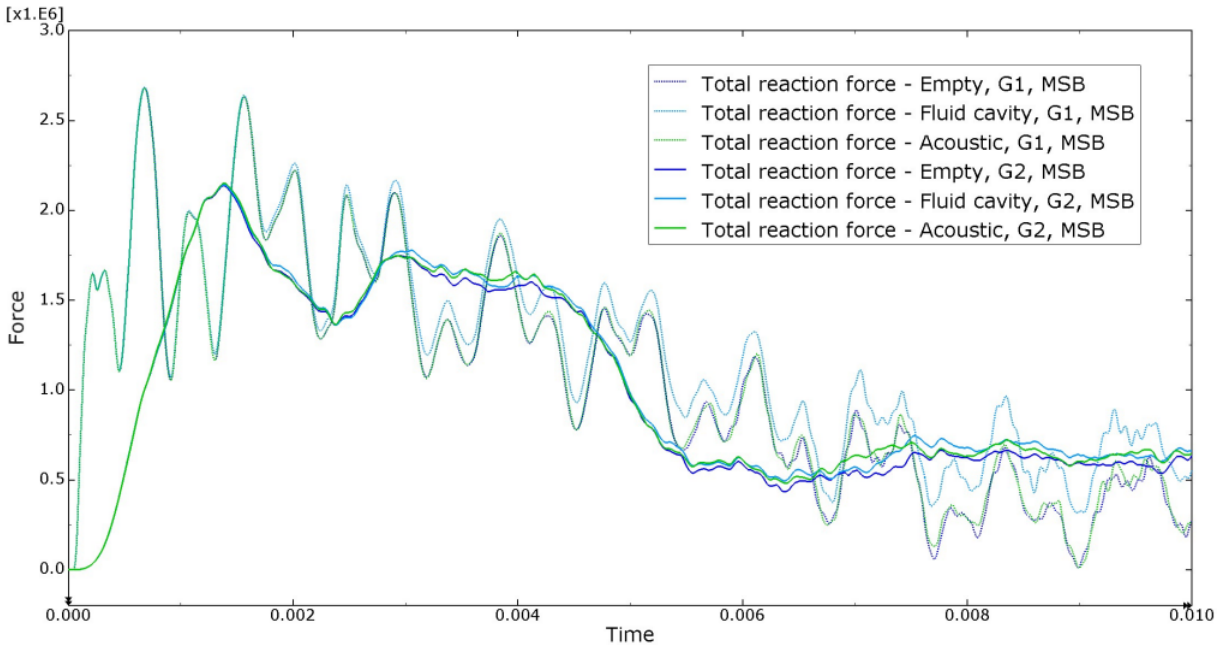

Figure 4.33: Compilation of the reaction forces computed for the various models of the air, shown for the MSB load

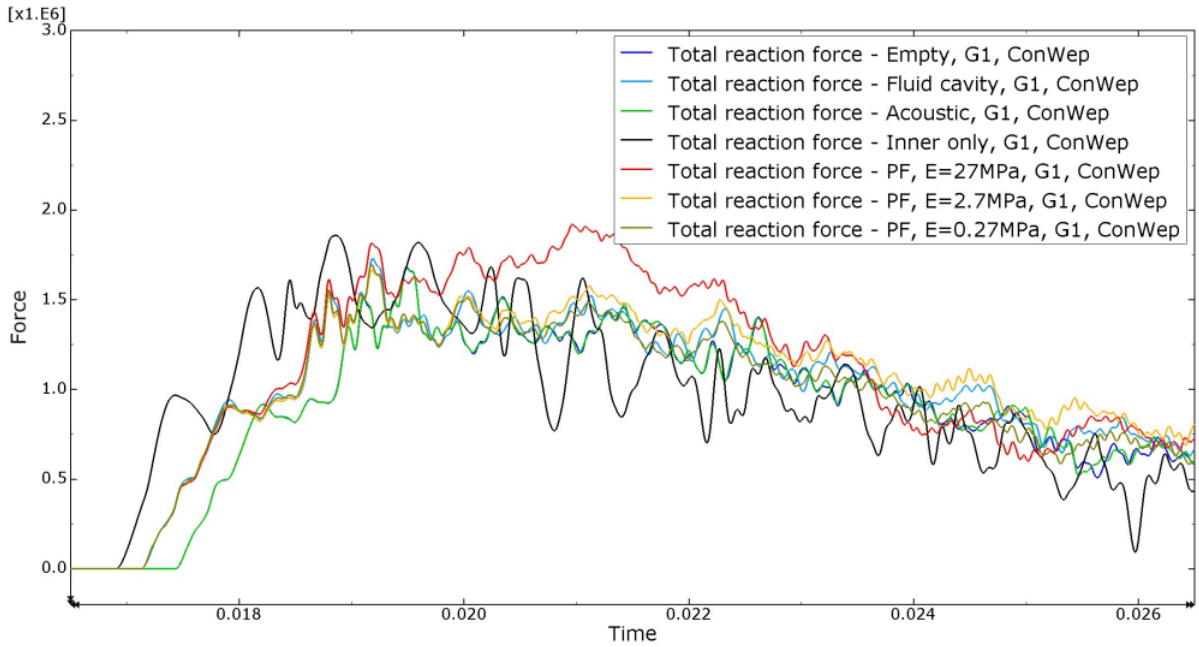

Figure 4.34: Compilation of the reaction forces for all the models of the plate–wall element, shown for the ConWep load

larger reaction force. Apart from this, the sizes off the reaction forces of the several models are similar.

In Figure 4.35, the reaction forces of the ConWep loaded column– wall element are shown for the different core layers. As for the MSB loaded wall, the solid wall shows the largest reaction forces. The rest of the models show similar results to each other, with the air models showing reactions slightly higher than the foam models.

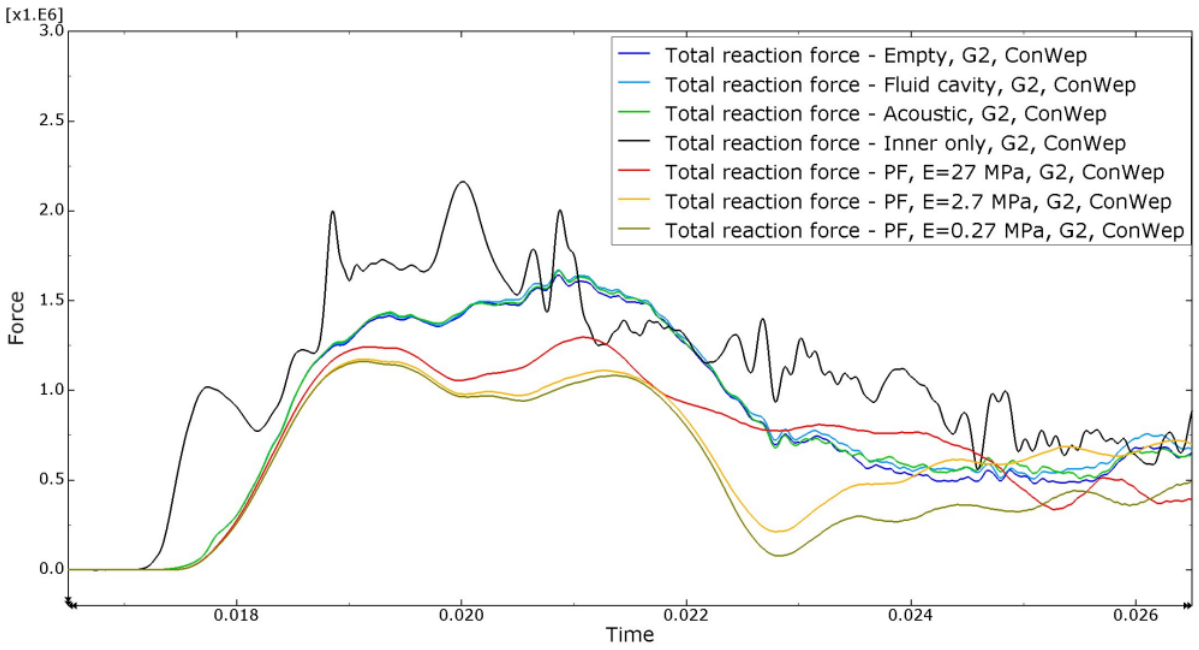

Figure 4.35: Compilation of the reaction forces for all the models of the column–wall element, shown for the ConWep load

To easier be able to compare the different geometries, the results of the plate- and column–wall elements were plotted together. In Figure 4.36, the reaction forces when only the inner walls were modelled are shown. The curves for the reaction forces for the plate- and column–wall elements correspond well. The column–wall element leads to the largest reaction force.

In Figure 4.37, the reaction forces for the models with phenolic foam as the core material are shown. Generally, the plate–wall element leads to the largest reaction forces. It can also be observed that the reactions for the different core materials correspond to each other initially, but deviate after a time. After that the weakest foam leads to the smallest reaction force, and the stiffest lead to the largest.

In Figure 4.38, the reaction forces for the models with air as the core material are shown. The reaction forces for the air models for the plate- and column–wall elements are quite equal. It can also be noted that the three ways of modelling air correspond well to each other.

4.5 Stress and Strain

For the reinforcement, it can be important to check that the stresses and strains are not unreasonable, and also how the distribution over the models look. For this, the principal stress S11, the stress in the lengthwise direction of the bar, as well as the plastic strain, was chosen. In the following plots, the values are presented for both the vertical- and horizontal part of the reinforcement mesh. In Figure 4.39, the stress–strain relationship for the reinforcement in the inner wall is presented, and in Table 4.2, the values are presented in a table form.

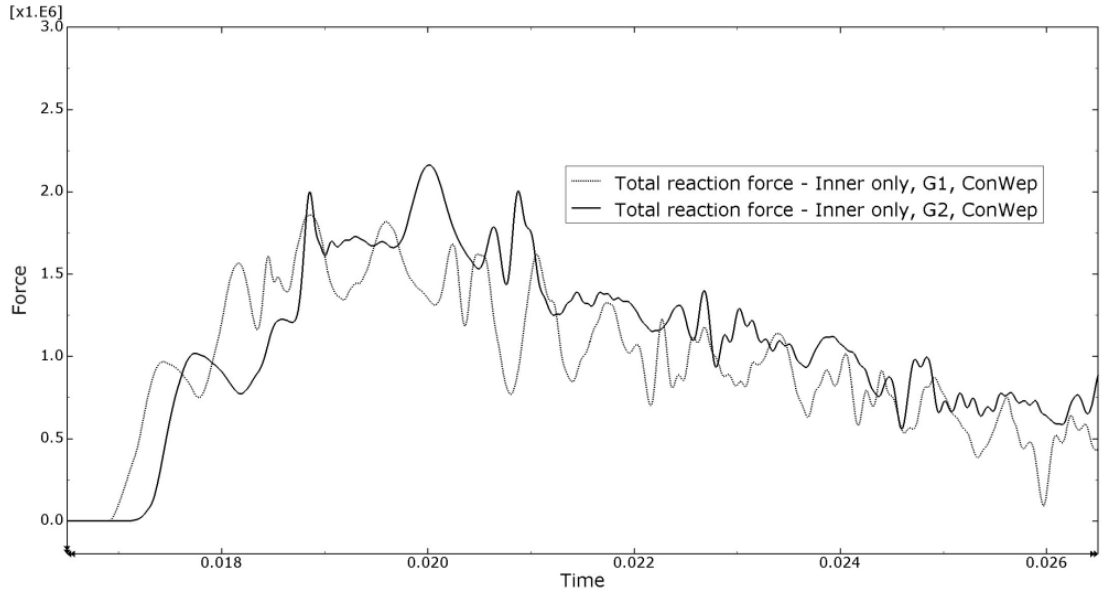

Figure 4.36: Compilation of the reaction forces for the inner slab only, the plate- and column–wall elements, shown for the ConWep load

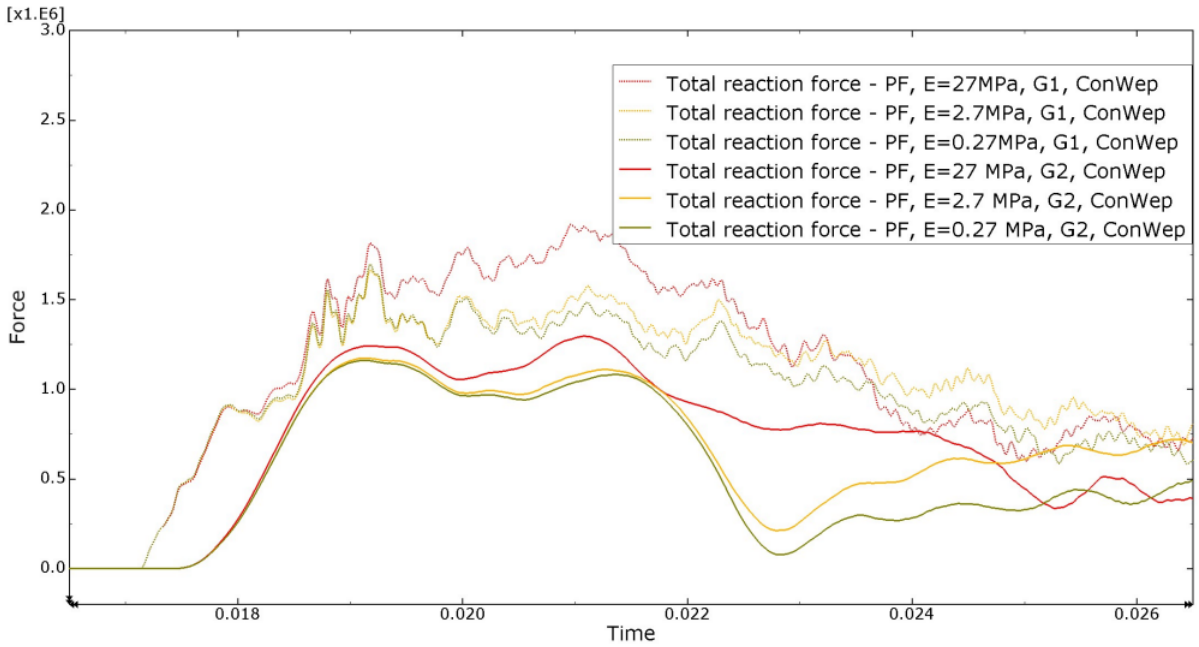

Figure 4.37: Compilation of the reaction forces when the core is made up of phenolic foam of different stiffnesses, for both the plate- and column–wall elements, shown for the ConWep load

From the figure and table, it can be observed that the largest stress–strain relationship was shown for the solid wall. Another notation is that the highest values all are gained for the column–wall element.

In Figure 4.40, the stress–strain relation is presented for the reinforcement mesh in the outer wall. In Table 4.3, the values are presented in table form. From these, it

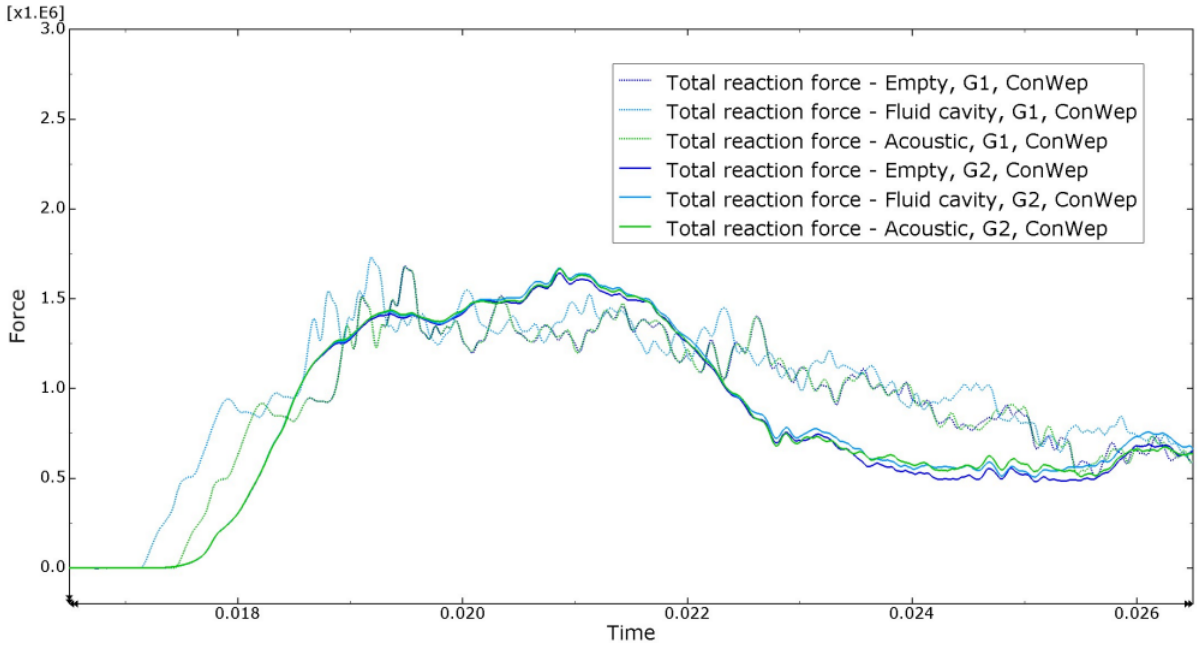

Figure 4.38: Compilation of the reaction forces when the core is made up of air, shown for the ConWep load

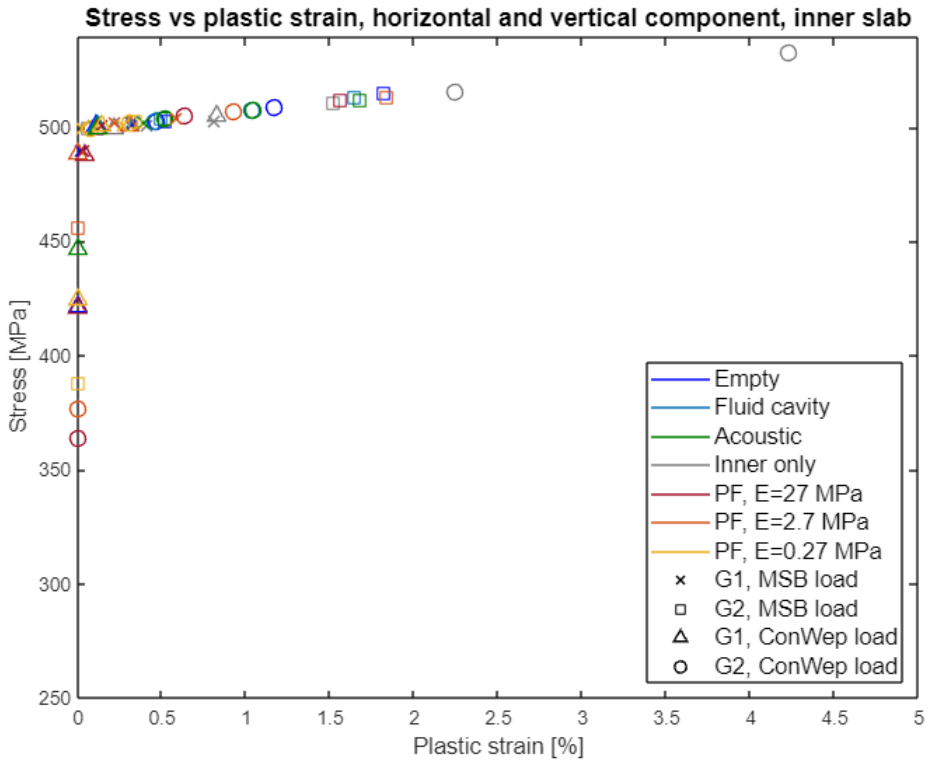

Figure 4.39: The stress and plastic strain for the inner slab, both the vertical and horizontal value, shown for all the wall- and load models

can be observed that the values are generally higher than for the inner wall.

Table 4.2: Stresses and plastic strains for the inner slab, shown for all the wall- and load models, stress/strain

Model	MSB [MPa / %]		ConWep [MPa / %]	
	G1	G2	G1	G2
Inner only	503/0.81	511/1.52	505/0.83	533/4.23
PF, $E = 27$ MPa	501/0.15	512/1.56	488/0.05	505/0.64
PF, $E = 2.7$ MPa	504/0.59	513/1.84	501/0.31	507/0.93
PF, $E = 0.27$ MPa	501/0.27	503/0.35	501/0.15	502/0.31
Empty	501/0.32	515/1.82	501/0.11	509/1.17
Fluid cavity	502/0.33	513/1.65	501/0.15	508/1.04
Acoustic	502/0.40	512/1.02	500/0.12	508/1.05

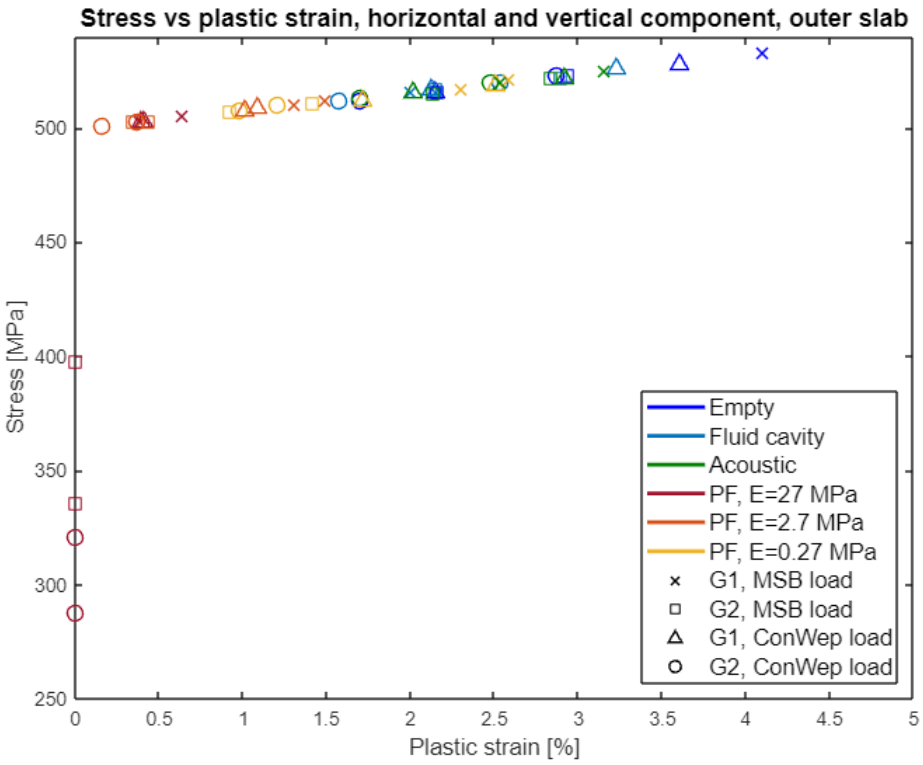

Figure 4.40: The stress and plastic strain for the outer slab, both the vertical and horizontal value, shown for all the wall- and load models

Table 4.3: Stresses and plastic strains for the outer slab, shown for all the wall- and load models, stress/strain

Model	MSB [MPa/%]		ConWep [MPa/%]	
	G1	G2	G1	G2
PF, $E = 27$ MPa	505/0.64	398/0.00	503/0.41	321/0.00
PF, $E = 2.7$ MPa	512/1.49	503/0.44	509/1.09	503/0.37
PF, $E = 0.27$ MPa	521/2.59	511/1.42	519/2.51	510/1.21
Empty	533/4.10	523/2.94	528/3.61	523/2.87
Fluid cavity	516/2.15	522/2.90	526/3.23	520/2.54
Acoustic	525/3.16	522/2.84	522/2.92	520/2.48

5 Discussion

The purpose of this master's dissertation was to investigate if the sandwich design is preferable to a solid wall when the wall is affected by a blast load. Sandwich walls with two different geometries, and several different core materials were analysed regarding which design lead to the least damage to the load carrying inner wall. The results show that the sandwich design is better than a solid wall for withstanding blast loads. They also show that overall, the design with columns is the most advantageous. When the core material is considered, air is the best, as long as the outer wall does not hit the inner wall – since this allows the outer wall to deflect and plasticise to its limit, and thus will not transfer this energy into the inner wall. However, it is not realistic to design the walls only for the risk of explosions, and therefore insulation will be included in the element. The analysis showed that for foam materials, a lower stiffness leads to a behaviour most similar to air, which is beneficial.

Choosing a sandwich wall as opposed to a solid wall automatically leads to some advantages. Firstly, this means that the stand-off distance increases, which leads to a decrease of the energy affecting the wall. Secondly, it leads to a larger mass, which means that a larger amount of energy is needed for moving it, leading to a reduction of the load affecting the construction [2].

There are some simplifications that have been made for this analysis. Firstly, no shear studs were considered in the design, and secondly, it was assumed that the inner- and outer wall were connected by stiff elements. Most importantly is that there was no experiment to verify the modelling against, and also no possibility to do own experiments and measurements on the materials, and thus, only data from earlier documented experiments and studies could be used.

5.1 Energy

The energies can be used both to clarify that there is equilibrium for the result, and also to investigate how much energy is absorbed by the structure. Due to this, large values of the total internal- and external energies show that a larger part of the energy from the blast was absorbed by the structure, which means that less energy will be transferred to the rest of the building.

Table 4.1 shows that the models of the column–wall element, for when only the inner wall is considered, has energies that show problematic tendencies. If this is considered when analysing the other parameters, this could be due to the connection between the slab and the column getting such large complications – in the shape of for example tensile damage and stress – in combination to how nonlinear the problem is that leads to the material model giving incorrect results.

In Figure 4.3, it can be observed that the energy for the phenolic foam with a stiffness of 27 MPa is the lowest, even lower than for the solid slab, showing that a high stiffness of this foam is not beneficial, even compared to a solid wall. If the stiffness is reduced by a factor of 10, into 2.7 MPa, the energy is raised considerably, showing that the softer behaviour is advantageous. If the stiffness is reduced by a factor 10 once more, into 0.27 MPa, the energy is raised higher again, showing that the amount of energy that can be absorbed by the wall is – in this case – closely tied to the stiffness of the foam. This was made clearer by the plot showing how the internal energy varied with the foam stiffness, Figure 4.6. This showed that the reduction of capacity for energy absorption was reduced between 11% and 22% when the stiffness was 2.7 MPa compared to 0.27 MPa, and between 44% and 62% when the stiffness was 27 MPa compared to 0.27 MPa. Since the foam stiffness was the only parameter varied between these models, with everything else being fixed, this shows that the stiffness has a large impact on how the whole wall can absorb energy.

The energy of the three air models act similarly in the beginning of the analysis, as is shown in Figure 4.4, and reaches about an equal maximal energy level. After this, however, the model with acoustic elements starts to deviate by decreasing, while the others stay constant. The reason for this is likely that no energy quantities are computed for the acoustic elements, meaning that these will not be represented in the total energy balance [19].

In the comparison between the energies of the fluid cavity, phenolic foam with a small stiffness, and the solid slab, it can be observed that the difference between the energy levels of air and the foam is quite small, showing that if the foam has a weak stiffness, the outer wall and foam can plasticise and deflect considerably, leading to a large absorption of energy.

In summary, what the energies can show is that a sandwich wall is better at withstanding blast loads than a solid wall – if the stiffness of the foam material is not too large. It also shows that the ideal material to have between the walls is air, but since other factors than robustness against explosions also influence the choice of wall design, the wall will not be built in that way. However, the analyses also showed that if the stiffness of the foam is low, in this case 0.27 MPa, the energy absorption capabilities are almost level with the air, meaning that this material also would lead to a wall with good properties for withstanding explosions.

5.2 Displacement

The displacements can be useful for two reasons. For the inner wall, a large deflection is problematic, since this is the load carrying wall. If this obtains a large displacement, the normal force can lead to instability and large moments that the wall is not designed to withstand. The outer wall, however, is not load carrying, and can thus be sacrificed. Due to this, a large displacement is advantageous for the outer wall, since the larger the deflection – in combination with the stiffness – the more energy can be absorbed, as was earlier shown in Figure 2.8.

Overall, the two ways of applying the load lead to similar results, with the resulting deflections in the same order. If the plots for the inner walls when the core is made of phenolic foam, Figures 4.7 and 4.11, are compared to each other, it can be observed that, for both geometries, the solid slab is the worst affected. This is followed by the foams in order stiffest to weakest. One can also observe that for both load applications, the column–wall element leads to reduced displacements compared to the plate–wall element. This is logical, due to the fact that the column–wall element is stiffer, and thus will not get as large displacements.

The outer slabs, when considering the foams as core materials, Figures 4.8 and 4.12, show that the size of the deflections are in the opposite order than for the inner walls. The largest displacement is obtained when the stiffness of the foam is the lowest, and the smallest when the stiffness is the highest, showing that the outer wall can deflect more when the resistance from the foam is lesser.

The deflections of the inner walls when the core consists of air, Figures 4.9 and 4.13, shows that these are close to zero, and thus negligible. Compared to the foam of weak stiffness, it can be observed that the deflections of the inner walls are quite equal.

The deflections of the outer slab when the core consists of air, Figures 4.9 and 4.13, shows that all three ways of modeling the air show similar results, i.e. that the wall will deflect considerably. There is some variation between the methods, which is shown by the difference in how much the outer wall deflects. For both methods of applying the load, the model with the empty cavity shows the largest deflections, followed by the fluid cavity and the acoustic elements. The fact that deflections of the model in which the air was not considered are the largest is reasonable, due to the fact that the air, when it is modelled, leads to a certain resistance, making it harder for the outer slab to move through the medium.

In summary, the deflections show that in order to get the smallest deflections to the inner wall, the core material should be air or phenolic foam of a low stiffness – in this case with a Young's modulus of 0.27 MPa. However, the results also show that even if a higher stiffness is used for the foam, the inner wall deflects less than a non sandwich wall. It also shows that the geometry that leads to the smallest deflections is the column–wall element.

5.3 Tensile Damage

The tensile damage that the concrete has accumulated due to the blast load is important to take into consideration. By visualising the damage, cracks and problematic zones can be noted, and an evaluation can be done of how damaged the wall is to see if it risks failing completely, or can keep being utilised. How the wall is damaged is also important to take into consideration, since the wall mainly transfers the load through the parts of the concrete on the outside of the window opening. Thus, if this part is damaged, it is problematic for the wall element.

The aim is to protect the inner, load carrying, wall from damage and failure. However,

the outer wall is not load carrying, and can thus be sacrificed to protect the inner wall. Due to this, it is seen as positive for the outer wall to have much damage, while this is negative for the inner wall.

From the results, it can be observed that there is a high risk that the solid wall, as well as the walls with phenolic foam cores of stiffness 27 or 2.7 MPa, might fail, especially for the plate–wall element. There is simply too much damage to the inner wall, especially on the back, for it to be utilised as before the explosion. When the stiffness of the foam is smaller, in this case 0.27 MPa, the damage to the inner wall is reduced considerably, showing that it is possible that this wall might be utilised as before. It can also be noted that the damage to the outer wall increases for a decreased stiffness.

For the air models, the results look very similar to each other. In Figures 4.19 - 4.21, for the plate–wall element, the damage to the inner wall is centered around the corners of the windows, with some additional damage on the front. The outer wall is considerably damaged, due to the fact that it can deform and plasticise to its full capacity, with no layer stopping it. The same can be seen for the column–wall element, in Figures 4.26 - 4.28, with the difference being that there is some more damage to the inner wall, mostly in the center, and where the slab is connected to the column. Overall, the column–wall element shows less fully developed damage than the plate–wall element does, showing that this design is more resistant to blast loads when the damage is considered.

In summary, the plots of the tensile damage show that the core material that leads to the least damage to the inner wall is when no insulation is used, only air, but it also shows that when using foam of a low stiffness, the result is quite similar compared to air. It also shows similar trends for the plate- and column–wall element, but shows that the connection between the column and the slab is a weak point in the design, since this will be subjected to large stress concentrations, and thus making it critical to design this for ductile behaviour. Irregardless of this, the column–wall element accumulates less damage than the plate–wall element, especially for the critical parts of the wall.

5.4 Reaction Force

The reaction forces transferred to the rest of the building are also relevant to analyse, since they will show how the rest of the building might be affected by the explosion.

From the reaction forces, it can be observed that when the load is applied via the ConWep module, the sizes are generally lower. It also leads to the forces being more similar in size between the different core materials compared to when the load is applied as a pressure. The reason for this might be that the MSB method of applying the load is a simplified model, that leads to conservative loads, while use of ConWep leads to data from real explosions being used, and thus leading to more realistic results.

For both methods of applying the load, and for both geometries, the reaction force

of the solid wall increases the most of all in the beginning. This is likely due to the stiffness of the inner wall being larger than for the outer wall – since this is thinner. This leads to the deformation capacities not being the same, since the weaker structure can deform more before reaching failure.

The distribution of the results are varied among the models. For the plate–wall element, after the initial phase, all cores lead to similar reaction force sizes. For the column–wall element, the reaction force gained by the solid wall is considerably larger than for the other models. The reason for this is likely that the ratio of the stiffness between the inner- and outer wall is larger for the geometry with the columns.

What can be observed by comparing the foams of different stiffnesses to each other, Figures 4.32 and 4.37, is that, initially, the reactions act the same, but after about 1.5 ms for the plate–wall element, and after the first peak for the column–wall element, they start to diverge. Then the reaction forces of the foams of the lowest stiffness starts to decrease more than the ones of higher stiffness, showing that the force diminishes at a higher rate when the stiffness is lower.

The three ways of modelling air show very similar reaction forces when compared to itself within the same loading method and geometry. This shows that when the reaction forces are the sought parameter, there is no need to model the air if this is not needed for another result, since the analysis without the air added runs faster, and leads to reaction forces of equal size and behaviour.

In summary, the reaction forces generally show that the worst wall to use is the solid one, showing that it is preferable to use a sandwich design. The core material leading to the lowest reaction forces for all the models is the phenolic foam of low stiffness. This is different from what the other results have shown, which is that air is the best core material. When the geometry is considered, the column–wall element led to the smallest reaction forces.

5.5 Stress and Strain

The stresses and plastic strains in the reinforcement meshes were checked, to see that they were not too large, or showing unreasonable behaviours. What can be observed from Figures 4.39 and 4.40 is that the points on the stress strain diagram follow a reasonable curve, with no outliers.

For the inner wall, it can be observed that the highest stress and strain was reached for the solid wall. The models reaching the highest values can also be noted to be of the column–wall element. For the outer wall, the stresses and strains are generally higher than for the inner wall. A pattern that can be noted is that the models with air overall reach higher stresses and strains than the models with phenolic foam, with the phenolic foam of the lowest stiffness reaching the highest of these models. This corresponds to the other results shown.

5.6 Comparisons and Compilation

In this section, the correlations between the results, and also the conclusions drawn from these are going to be discussed.

Generally, it could be observed that loading the wall with a pressure load calculated from MSB led to larger reactions than loading the wall by use of the ConWep module. However, the order of how well the wall types work when loaded by the blast is generally the same.

The energies showed that the best core filling is air, but that phenolic foam of a low stiffness is almost as effective. Comparing the energy plots to the tensile damage showed that when the plastic dissipation energy stabilises, and stays approximately constant, the walls have accumulated the most of its damage, which also stays about constant after that time.

From the displacement plots, it could generally be observed that the column–wall element led to smaller displacements for both the inner- and outer wall compared to the plate–wall element. It could also be concluded that the best core filling is air or phenolic foam of a low stiffness. These cores lead to the inner wall getting negligible displacements, which is positive, since this is the load carrying wall. For the outer wall, it could be seen that the displacements became considerable when the core material was air or low stiffness foam. This can also be compared to the damage plots, in which it can be observed that the outer walls of these models accumulated much damage from the blast.

In the case of the reaction forces, the results varied some, with some models showing that foam is the best core material independently of the stiffness, and with some showing that all core materials lead to similar forces. Over all the models, however, it could be seen that the foam of the lowest stiffness is the one that reduces the reaction force the fastest, showing that this is the best stiffness of the three tested. It also showed that the design with columns is favorable, since this results in smaller reaction forces overall.

The stress and plastic strain diagrams corresponds to the deflection and damage plots. It can be observed that for the outer wall, the models with the largest deflections and the most damage also get the highest values of stress and plastic strain.

6 Conclusions and Further Studies

6.1 Conclusions

Are sandwich elements favourable in blast loading situations, and what design is in that case the most favourable?

- Yes, sandwich elements are favourable compared to solid walls with the same load bearing part, for most core materials.
- The most favourable concrete design is to use a design in which the wall slabs are strengthened by columns.
- The most favourable core material is air or foam of a low stiffness. The most important thing is for the outer wall to be able to deform without encountering much resistance.

What methods of analysis are suitable for answering the above questions?

- Explicit dynamic analysis. Also the implicit method has been tried, but due to the non-linearity it is after a while almost impossible to find equilibrium, which makes the method inefficient, or even useless.
- For the air, all three of the versions; fluid cavity, acoustic elements and an empty cavity, led to similar results.
- For the loads, the results differed when the MSB load was used compared to the ConWep module, likely due to the fact that the MSB method is simplified, and ConWep is based on real explosion data.

6.2 Further Studies

Examples for further studies are presented below.

- Investigating more and different designs, both for the concrete and the core, such as adding one more outer wall.
- Varying other parameters than Young's modulus, such as the density or the compressive strength, for the foam to see how large of an impact these have.
- Investigating what design is the most advantageous for explosions with a smaller stand-off distance.

- Investigating how the wall elements used in this report would manage if hit by a car or dropped during the construction stage.

Bibliography

[1] Swedish Civil Contingencies Agency. *Den robusta sjukhusbyggnaden - En vägledning för driftsäkra sjukhusbyggnader*. Tech. rep. MSB1693. Karlstad, 2021.

[2] Morgan Johansson and Leo Laine. *Bebyggelsens motståndsförmåga mot extrem dynamisk belastning - Del 3: Kapacitet hos byggnader*. Tech. rep. MSB142. Karlstad: Swedish Civil Contingencies Agency, 2012.

[3] Robert Studziński, Tomasz Gajewski, Michał Malendowski, Wojciech Sumelka, Hasan Al-Rifaye, Piotr Peksa and Piotr Sielicki. "Blast Test and Failure Mechanisms of Soft-Core Sandwich Panels for Storage Halls Applications". In: *Materials* 14.1 (2021), pp. 1–14.

[4] Yang Yang, Arash Soleiman Fallah, M. Saunders and Luke A. Louca. "On the dynamic response of sandwich panels with different core set-ups subject to global and local blast loads". In: *Engineering Structures* 33.10 (2011), pp. 2781–2793.

[5] Morgan Johansson. *Luftstötvåg*. Tech. rep. MSB448. Karlstad: Swedish Civil Contingencies Agency, 2012.

[6] Morgan Johansson and Leo Laine. *Bebyggelsens motståndsförmåga mot extrem dynamisk belastning - Del 1: Last av luftstötvåg*. Tech. rep. MSB449. Karlstad: Swedish Civil Contingencies Agency, 2012.

[7] ConWep. *ConWep – Collection of conventional weapons effects calculations based on TM 5-855-1, Fundamentals of Protective Design for Conventional Weapons*. Tech. rep. Vicksburg, USA: U.S. Army Engineer Waterways Experiment Station, 1992.

[8] *Abaqus/CAE User's Guide*. 2016.

[9] *Abaqus Theory Guide*. 2016.

[10] Milad Hafezolghorani, Farzad Hejazi, Ramin Vaghei, Saleh Jafaar and Keyhan Karimzade. "Simplified Damage Plasticity Model for Concrete". In: *Structural Engineering International* 27.1 (2017), pp. 68–78.

[11] Swedish Institute for Standards. *Eurocode 1: Actions on structures - Part 1-1: General actions - Densities, self-weight, imposed loads for buildings*. Tech. rep. SS-EN 1991-1-1. Stockholm, 2002.

[12] S.M Anas, Mehtab Alam and Mohammad Umair. "Effect of design strength parameters of conventional two-way singly reinforced concrete slab under concentric impact loading". In: *Materials Today: Proceedings* 62.4 (2022), pp. 2038–2045.

[13] Swedish Institute for Standards. *Eurocode 2: Design of concrete structures – Part 1-1: General rules and rules for buildings*. Tech. rep. SS-EN 1992-1-1:2005. Stockholm, 2005.

[14] Tord Isaksson and Annika Mårtensson. *Byggkonstruktion: Regel- och formelsamling*. 4th ed. Studentlitteratur AB, 2020.

[15] Vincent Coppock, Ruud Zeggelaar, Hiroo Takahashi and Toshiyuki Kato. “Phenolic Foam”. Pat. US 8772366 B2. 2014.

[16] Swedish Institute for Standards. *Thermal insulation products for buildings – Factory made phenolic foam (PF) products – Specification*. Tech. rep. SS-EN 13166:2012+A2:2016. Stockholm, 2016.

[17] C Mougel, T Garnier, P Cassagnau and N Sintes-Zydowicz. “Phenolic foams: A review of mechanical properties, fire resistance and new trends in phenol substitution”. In: *Polymer* 164 (2019), pp. 86–117.

[18] Matteo Colombo, Paolo Martinelli, Roberto Zedda, Aldino Albertelli and Nicola Marino. “Dynamic response and energy absorption of mineral–phenolic foam subjected to shock loading”. In: *Materials Design* 78 (2015), pp. 63–73.

[19] *Abaqus Analysis User’s Guide*. 2016.

[20] Lars Wadsö. *Construction Materials Science*. KFS i Lund AB, 2021.

[21] Niels Ottosen and Hans Petersson. *Introduction to the Finite Element Method*. Pearson Education Limited, 1992.

[22] Anil K. Chopra. *Dynamics of Structures: Theory and Applications to Earthquake Engineering*. 5th ed. Pearson Education Limited, 2020.

[23] *Getting Started with Abaqus/CAE*. 2016.